Student thesis series INES nr 677

Modelling dynamic wood density in LPJ-GUESS

Anna-Kristina Voss

2024
Department of
Physical Geography and Ecosystem Science
Lund University
Sölvegatan 12
S-223 62 Lund
Sweden

Anna-Kristina Voss (2024).
Modelling dynamic wood density in LPJ-GUESS
Title of thesis in Swedish
Master degree thesis, 30 credits in Physical Geography and Ecosystem Science
Department of Physical Geography and Ecosystem Science, Lund University

Level: Master of Science (MSc)

Course duration: *January* 2024 until *June* 2024

Modelling dynamic wood density in LPJ-GUESS

Anna-Kristina Voss

Master thesis, 30 credits, in *Physical Geography and Ecosystem Science*

Supervision:

Annemarie Eckes-Shephard
Lund University

Stefan Olin
Lund University

Exam committee:
Tom Pugh, Lund University
Camille Volle, Lund University

Contents

Acknowledgments

I am truly grateful to my supervisors, Annemarie and Stefan, for their unwavering support and dedication to this project. Their guidance has often opened my eyes to new opportunities and improvements, and has reminded me of the essential aspects. Without their initiative and encouragement, I would not have ventured into tree ring modelling. I am also thankful to Hao Zhou for sharing his model code with me and to Patrick Fonti for his efforts in providing me with data from the validation sites.

I want to express my gratitude to Daniël, my previous opponent, for his great feedback on my early submissions and my other proofreaders, Maria, Ted and Juli. For technical support and feedback on the design, I am sincerly grateful to Sasha. Lastly, I want to express my special thanks to all the people emotionally supporting me through the past months, Lotta, Leonie, Elsa, Edith and especially Tibak.

Abbreviations

ANPP	Annual Net Primary Productivity
DGVM	Dynamic Global Vegetation Model
EW	Earlywood
GSS	Growing Season Start
LPJ-GUESS	Lund-Potsdam-Jena General Ecosystem Simulator
LW	Latewood
PFT	Plant Functional Type

Summary

1 | Introduction

Forest ecosystems play a vital role in regulating the global climate system and are known for their role in offsetting anthropogenic greenhouse gas emissions (Friedlingstein et al., 2022). Globally, forests are a net carbon sink of an estimated 7.6 GtC per year (Harris et al., 2021). Trees are crucial elements of forests by absorbing carbon dioxide emissions through photosynthetic activity and storing carbon in wood (Pan et al., 2011, IPCC, 2019). A big part of understanding just how much carbon trees can store comes down to how they build their wood over time. A combination of various mechanisms dictates both the quantity and quality of newly formed woody tissue, with wood density serving as an important determinant of carbon storage capacity (Chave et al., 2019, Mo et al., 2024). Despite its significance, wood density is frequently overlooked as a variable in dynamic global vegetation models (DGVMs), which are computational tools used to simulate the dynamics of vegetation and its interactions with the environment on a global scale. This oversight results in the exclusion of wood density's response to environmental controls like temperature, affecting the accuracy of future projections.

Not considering the variability of wood density in trees can lead to uncertainties in the estimations of the quantity of stored carbon and the residence time of carbon in a tree (Mo et al., 2024, Yang et al., 2024). Further, wood density is integral to tree mechanics, nutrient storage and water transport and can be part of a trees strategy in terms of resilience (Ackerly, 2003, Chave et al., 2009, Anderegg et al., 2016). Consequently, including how wood density responds to the environment in vegetation models is of importance for accurately estimating carbon storage and growth dynamics in forests. The objective was to develop a dynamic wood density model and integrate it into the DGVM Lund-Potsdam-Jena General Ecosystem Simulator (LPJ-GUESS). This thesis aimed to enhance the understanding of how environmental influences shape wood density dynamics and, consequently, how it affects dynamics in modelling forest ecosystems.

1.1 | Background

1.1.1 | Wood formation

Wood formation is the process of expanding wood tissue in diameter and height of the stem through which carbon is incorporated into long-standing biomass. Carbon uptake and longterm storage is, due to the anthropogenic increase in carbon in the atmosphere, an ecosystem service of high interest. With approximately 50% of carbon in trees being stored in woody tissue and wood being the carbon pool of a tree with the slowest turnover rate, the process of wood formation

determines the carbon storage abilities of trees (Mo et al., 2024). Wood formation occurs in the cambium, the actively dividing layer of cells on the outside of the stem (Catesson, 1994, Funada, 2008). In temperate and boreal climates wood formation is bound to a growing season and goes through dormancy. Cambial activity follows a seasonal pattern adapted to the climate (Funada et al., 2016), with reactivation controlled by temperature (Oribe and Kubo, 1997, Oribe et al., 2001, Gričar et al., 2006, Begum et al., 2013, Cuny et al., 2019).

The characteristics of formed wood exhibit spatial and temporal variations. Spatial differences are influenced by factors such as species composition, biodiversity levels, and climatic conditions (Mo et al., 2024). Meanwhile, temporal variations arise from the specific growing conditions experienced by individual trees. These conditions are in temperate climates recorded in their tree rings. Tree ring formation progresses from spring to autumn, characterised by phases of cell enlargement and cell wall thickening. This leads to the formation of earlywood (EW) and latewood (LW) within a ring which determine the phenology of the formed wood. EW is formed in the early growing season, characterised by large-diameter tracheid cells with thin walls (Cuny et al., 2014) (Fig 1). What exactly controls the formation of EW is yet to be determined with certainty (Cuny and Rathgeber, 2016, Cuny et al., 2019). Wider EW is often reported to correlate with water availability while density correlates partly positively with increasing temperatures and negatively with higher precipitation (Camarero et al., 2017, Bytebier et al., 2022). Frequently reported are also compensatory effects during EW formation, where trees compensate for shorter growing seasons with higher cell enlargement rates and vice versa, which reduces the impact of environmental controls. Furthermore, the formation of EW is potentially limited by the available carbon based on early growing season conditions, with higher investments of the tree in leaves and shoots (Friend et al., 2022). In the later growing season LW is formed consisting of cells narrower in diameter with thicker walls (Cuny et al., 2014) (Fig. 1). Formed LW is generally denser than EW. Temperature during the time of formation is a well-established determinant of LW and maximum density in a ring (Levanič et al., 2009, van der Maaten et al., 2012, Düthorn et al., 2016, Cuny et al., 2019, Boakye et al., 2023). LW is not limited by available carbon but rather LW growth limits carbon deposition into wood.

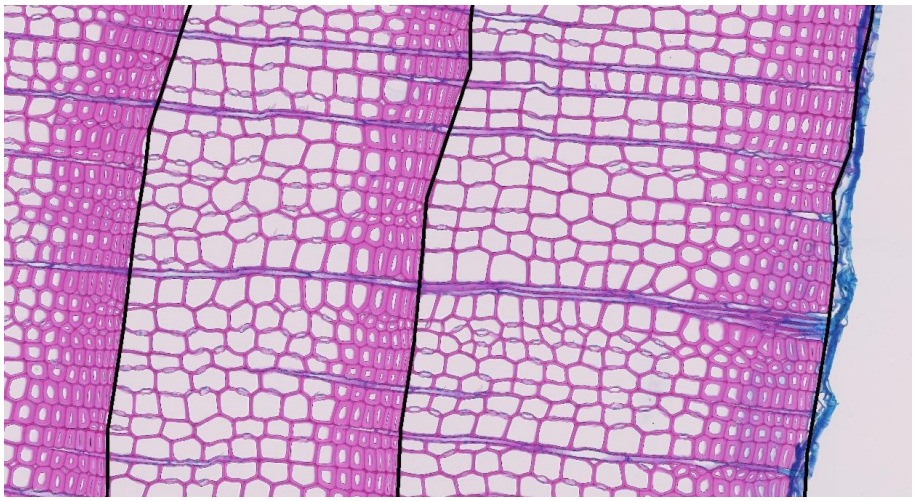

Figure 1: Microscope image of two annual tree rings of a European larch tree growing in Lötschental, Switzerland. Tree rings are separated by black lines with tree bark on the right with each tree ring consisting of earlywood cells which are bigger and primarily consist of lumen (white) and latewood cells which have significantly thicker cell walls (pink).

The densities of the formed EW and LW characterise the gradual increase in density throughout the ring, creating a common pattern. Wood density is low in EW and increases moderately with a transition from EW to LW visible from the steep increase in density (Fritts, 1976). Due to the complexity of wood formation and the various factors playing into it, environmental factors have been only shown to explain variations in width and density to a certain extent. A lot of non-environmental variance stems from tree internal processes and hormones but also individual properties such as age, height, and crown area (Rosell et al., 2017). Further environmental conditions seem to have ambivalent or indirect effects, additionally playing into variance that can not be explained by correlations between phenomena and variable (Cuny and Rathgeber, 2016). Wood density has shown to be spatially linked to climate conditions such that increasing latitude and altitude correlate with lower mean wood densities (Mo et al., 2024). Temperature is thereby the likely driver of higher mean wood density.

Besides carbon storage and biomass generation as topics of interest in the context of climate mitigation and forestry, wood density has several roles in trees. The quality of wood determines the mechanical support of trees, pathogen defence abilities, nutrient storage, water transport and drought tolerance (Ackerly, 2003, Chave et al., 2009, Cuny et al., 2019, Pretzsch et al., 2018). Wood density is also tied to mortality through resilience to i.e. storm breakage and recovery after disturbance. It helped explain observed variability in mortality with lower density being associated with higher mortality (Anderegg et al., 2016, Chao et al., 2008). It has been observed that trees with lower wood density are typically early colonisers. However, trees with higher wood density demonstrate superior recovery following disturbance (Mo et al., 2024). Furthermore, wood density has been shown to have an additional impact on carbon turnover

through mortality, thus affecting the forest carbon pool (Yang et al., 2024). Despite the evidence of various physiological roles, wood density is not yet mechanistically modelled and integrated in policy-relevant DGVMs.

1.1.2 | Modelling wood density

In general, modelling wood formation is not an unexplored field. Various models exist developed in different fields, of varying complexity and purpose. Different fields including forestry, dendroclimatology and plant physiology have been exploring wood formation models. Eckes-Shephard et al. (2022) summarised the historical development of models in the different fields and the existing wood formation models with their properties such as inputs, time scales and assumptions. Besides field and properties, models can also be divided into mechanistic and empirical models. Mechanistic models simulate underlying biological processes from which wood formation emerges, generally requiring complex equations and inputs. Empirical models rely on statistical relationships between properties of formed wood such as width or density and environmental variables. This project is a step towards a simple wood density model compatible for integration into DGVMs.

Mechanistic models for wood formation usually simulate the process on cell level. One popular example of a dendroclimatology model is the Vaganov–Shashkin model relying on environmental variables consisting of soil moisture, temperature and daylength as input (Vaganov et al., 2006). In the model simulated cells emerge, enlarge, and thicken based on environmental variables. It models tree ring width reasonably well but not wood density. A model by Drew and Downes (2015) relies on tree water, temperature and available carbon for modelling and was able to explain up to 80% of variations in tree ring average density. The model relies also on modelling cells and operates on a daily time step. A more recent approach by Friend et al. (2022) models cells both temporally and spatially to describe cells in different cell development phases governed by environmental impacts. It is able to reproduce the common density pattern in tree rings. Overall, mechanistic models can simulate density to some extent at site-level but they are complex and use many different inputs making them unsuitable for the use in DGVMs.

A range of studies developed empirical models based on correlations between environmental variables and density or width. Empirical density models are usually highly specialised to a location and are primarily used to explain local density variations. One of these models is for example developed by Van der Maaten et al. (2012) and was able to explain over 86% of variation in density. A more general approach using statistical relationships including mechanistic elements for modelling wood density is presented by Franceschini et al. (2013). Their developed model proposes to reproduce the common tree ring pattern by modelling minimum and maximum density and the time of transition from early, to transition to latewood as relative position in

the ring. It is assumed that density continuously increases from minimum to maximum density with different density increase rates for the three wood types. Based on this, linear equations are formulated for early, transition and late wood for the relative density increase in each part of the ring. However, the specific model parameters are calibrated to a local site and are not universally applicable. All empirical models depend on environmental conditions. The environmental factors used include temperature, various hydrological indices such as precipitation and vapour pressure deficit. As with the mechanistic models, the empirical models are site- or region-specific and therefore largely unsuitable for DGVMs.

Recently, more AI-based model approaches for modelling wood density on a global scale have been applied, such as those by Mo et al. (2024) and Yang et al. (2024). However, these studies are focused on modelling and explaining spatial variability both globally and locally. While these variations are often driven by climate and species, temporal variations are more directly related to the wood formation process itself. Therefore, modelling wood formation mechanistically is the best way to project into the future where known relationships, as included in empirical or AI-based models, might shift. Although these statistical models are useful in various applications, they are not well-suited for researching uncertain developments such as future scenarios subject to climate change. Due to the complexity and partly unknown processes related to wood formation (Eckes-Shephard et al., 2022), a completely mechanistic approach is nevertheless difficult to implement in DGVMs.

1.1.3 | European Larch in the Swiss Alps

This thesis developed a model of wood formation on larch data of Dahurian Larch, Siberian Larch and European Larch and was validated against European larch growing in the Swiss Alps at different elevations. The European larch (*Larix Decidua*) is closely related with the Dahurian Larch (*Larix gmelinii*) and the Siberian Larch (*Larix sibirica*). Studies showed that the three species are genetically and evolutionary closely related and categorize them as short bracted North Eurasian larch species (Semerikov and Lascoux, 1999, Wei and Wang, 2003, Wei and Wang, 2004, Gros-Louis et al., 2005). European larch is one of few deciduous conifers with a distribution in mountains in Central and East Europe. It primarily inhabits mountainous regions like the Alps, Sudetes, and Carpathians, with occasional presence in lowlands, notably in South Poland (Matras and Pâques, 2003). It spans approximately 500,000 hectares with a fragmented distribution. Due to its high tolerance to cold temperatures in winter, it is distributed often in high altitude along the upper tree line (Matras and Pâques, 2003). European larch is a fast-growing tree with low-shade tolerance and thereby counts as an early colonizer or pioneer tree. Furthermore, European larch is a long-lived tree which is highly adaptive under sufficient light conditions.

1.2 | Aim

The current wood density parameter in the DGVM LPJ-GUESS excludes the environmentally dependent variability in wood density. As the wood density affects allocation of carbon in LPJ-GUESS, a dynamic wood density has an impact on growth processes, which has been unexplored until now. To address this issue, this thesis aimed to make wood density vary as a function of the environment in a semi-mechanistic manner. The model consists of modelling temperature-dependent LW density and a growing season-dependent phenology of the tree ring. The model was validated with European Larch growing along an elevational transect in the Swiss Alps. The elevational transect is used to represent growth under different temperatures under otherwise similar climate. The first research question to be answered by the wood density model was:

Research Question 1:

- Can the general variability of mean annual wood density in European Larch (*Larix decidua*) across an elevational transect in the Swiss Alps be captured by modelling latewood density and tree ring phenology?
  - How does the model perform when only density of latewood is simulated?
  - How does modelling the phenology of formed tree rings contribute to the model performance?

The model containing only the temperature-dependent LW density was expected not to be able to capture the general variability of the tree ring density of the validation data. Spatial trends across the elevational gradient are likely reproduced due to the temperature-dependent latewood density function. Annual variations were expected to be less well represented as latewood density was found to explain only 40% of variations in total tree ring density in the data used for function construction (refer to a respective graph in appendix !!!). From this was concluded that the need for a phenology function is justified, which was expected to improve the model and better reflect the trend in annual tree ring density at different elevations. At higher altitudes, a later start to the growing season was hypothesised to lead to an overall shorter phase for EW formation leading to narrower EW width.

Hypothesis 1.1 & 1.2:

- The wood density model with only a temperature-dependent latewood density is not able to capture the general variability of mean annual tree ring density across elevations.
- The wood density model including both the latewood density function and the phenology function is able to capture the general variability of annual tree ring density across

elevations.

The implementation of the wood density model in LPJ-GUESS has a direct effect on tree growth within the model. Replacing the parameter with a modelled wood density adds a new capability to the model, the implication of which were explored in this thesis. To investigate the effect of variable wood density on tree growth dynamics, the following question were answered:

Research Question 2:

- How is tree growth of European Larch (*Larix decidua*) in the Swiss Alps along an elevational transect in LPJ-GUESS affected by replacing the wood density parameter with a dynamic wood density model?
  - How does the dynamic wood density model change the allocation of carbon between leaves and stem in a tree?
  - How is tree productivity affected across elevations?

The effect of a change in wood density on the model output was uncertain and had not been investigated before. The complexity of the processes and feedbacks represented in LPJ-GUESS further contribute to unclear output. No hypothesis could be formulated based on the effects of a change in wood density observed in nature, as wood density in the model is not a result of growth processes, but a variable that affects growth itself. Wood density is used in the allocation of carbon into leaves, roots and stem. As wood density is in the denominator of the allocation calculations, it was assumed that higher density results in lower height growth and lower carbon in leaves. Less investments in leaves by trees was connected to a reduced net primary productivity.

Hypothesis 2.1 and 2.2:

- The productivity of trees decreases with higher wood densities and less carbon is allocated to leaves.
- Higher wood density results in lower height of trees in LPJ-GUESS.

In conclusion this thesis aimed to address the inherent limitation of the non-variable wood density in LPJ-GUESS by replacing it with a dynamic model of wood density. The objective of the study was to create a model that captures how wood density responds to climatic variations and allows for environmental-dependent inter-annual variability in wood density that influences the growth processes in LPJ-GUESS.

2 | Methods

Due to the lack of a generalised wood density model that can be easily incorporated with LPJ-GUESS, the research initially focused on developing a model that could be easily coupled with the annual allocation scheme and is adaptable to fit a wider environmental range. Correlations and patterns between annual tree ring variables and environmental variables were identified from larch data across Europe and Russia. Based on these relations between variables, functions were developed that attempt to explain EW width based on the growing season onset. LW density is dependent on average summer temperatures, while LW width is non-linearly related to LW density (Fig. 2). EW density was set to a species-specific parameter for each of the three larch species. That partly compensated also for the different distribution of the trees per species (B1). The developed functions were validated against annual tree ring data from Lötschental, located in the Swiss Alps at four different sites across three elevations.

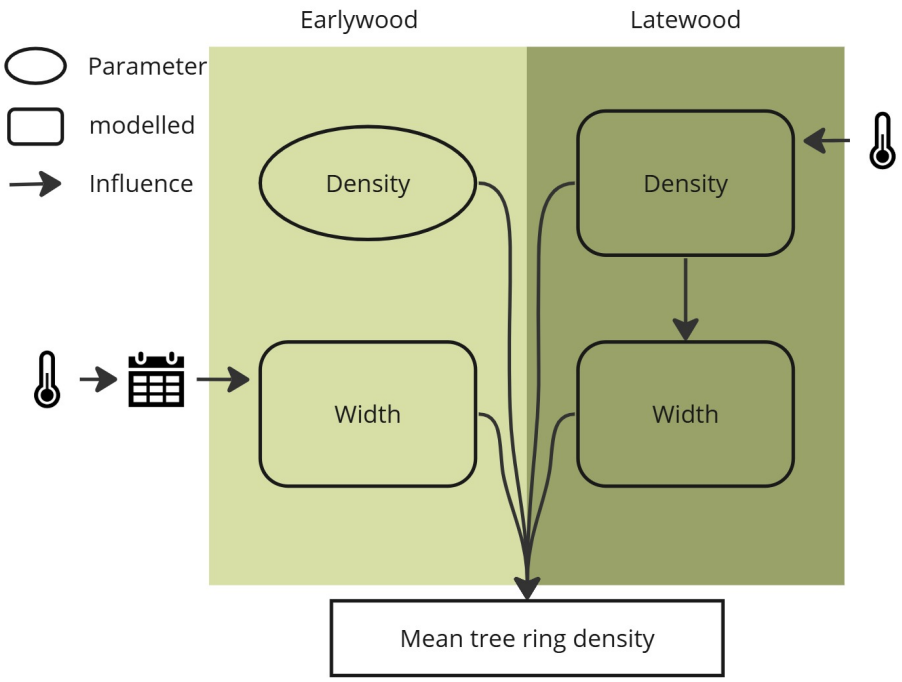

Figure 2: Conceptual illustration of the model consisting of earlywood and latewood with width and density as properties. Environmental factors playing into the model are mean July and August temperature for deriving the latewood density and the date of stem growth onset determined by the mean annual temperature.

The developed model was integrated into a version of LPJ-GUESS that includes topography. Outputs of the model from three different elevations (1300 m, 1700 m, 2000 m) for the standard LPJ-GUESS version and LPJ-GUESS with dynamic wood density (LPJ-GUESS-WD) were compared. For a detailed description of the data, used methods and LPJ-GUESS refer to Appendix A: Methods and Data (p. A-5) and Appendix B: Supplementary Material to Methods

and Data (p. B-1).

In this thesis, I developed a temperature-dependent, dynamic wood density model and integrated it into LPJ-GUESS. I constructed the LPJ-GUESS version by combining pre-existing versions to ensure it included elevation dependent temperatures and all necessary outputs to address the research questions. I was responsible for all data processing related to function-building, function-building itself, as well as model-data and model-model comparisons within the scope of this thesis. Preliminary research on a potential wood density model was initiated before the official timeframe of this thesis. This included part of the literature research and the development of early ideas using Norway spruce data, for which data processing scripts were written which I reused in this thesis. Additionally, the modification of the the modelled carbon allocation process to include dynamic wood density, along with the associated debugging, was carried out prior to the official thesis period. The changes in the allocation are from an allocation scheme provided by Stefan Olin. The topography version for LPJ-GUESS was contributed by Hao Zhou.

3 | Results

The developed dynamic wood density model was validated against observational data along a slope in the Lötschental for European larch including four sites across three elevations. With respect to the first research question, the performance of two mean tree ring density models was compared. When the mean annual tree ring density was modelled using only the dynamic LW density and a default phenology splitting the tree ring width into 70% EW and 30% LW, only 12% of the mean annual tree ring density across sites could be reproduced. Mean annual LW density was reproduced relatively well by 57% (Appendix A: Fig. 4). For both LW density and mean tree ring density, the model performance varied site dependent but with no recognizable factor causing the differences, as explained in Appendix A: Validation of the dynamic wood density model (p. A-11). When phenology emerges from modelled EW and LW width, 11% of mean annual tree ring density are reproduced. The fit of modelled EW and LW width to the observational data can be seen in Appendix A: Fig. 5 and can be read up in Appendix A: Validation of the dynamic wood density model (p. A-12).

From the dynamic wood density model validation in Lötschental can be concluded:

- Inter-annual mean tree ring density could not be modelled with a non-variable phenology.
- The emerging phenology as modelled in this thesis did not contribute to an improved mean tree ring density model.

To answer the second research question, the impact of dynamic wood density on the performance of LPJ-GUESS was assessed. In LPJ-GUESS including dynamic wood density (LPJ-GUESS-

WD), the annual mean tree ring density was higher at the lower elevations (1300 m & 1700 m) than in the standard LPJ-GUESS version and stayed in the same order of magnitude as the wood density parameter at an elevation of 2000 m (shown in Appendix A, Fig. 7). Besides at the end of the analysed time period, little tree growth occurred at the highest elevation combined with the little deviation from the wood density parameter leading to it being primarily excluded from the output analysis.

At mid-elevation, annual net primary productivity was on average higher in LPJ-GUESS-WD than in the standard LPJ-GUESS (Appendix A: Fig. 8a). The same applies to the amount of carbon in leaves and sapwood. At low elevation, the trend was not consistent. Productivity as well as the stored carbon in leaves was slightly lower in LPJ-GUESS-WD compared to the standard LPJ-GUESS. Carbon in sapwood was at low elevation higher in LPJ-GUESS-WD than in the standard version. Mean heights of trees across the time period were primarily greater in the standard version of LPJ-GUESS (Appendix A: Fig. 8b). Excluding age structure effects, trees in LPJ-GUESS-WD had lower mean heights in all age groups and at all elevations of up to 19% at age 80 at low elevation. This is described and visualised in greater detail in Appendix A: Comparison of LPJ-GUESS-WD to the standard LPJ-GUESS (p. A-13).

With regard to the second research question, it can be stated that higher wood density does not necessarily have a uniform effect, but based on the results, was concluded:

- An increase in mean stem wood density correlates with changes in productivity and the amount of carbon in leaves but no trend can be found based on the analysed sites.
- Higher mean stem wood density can be associated with smaller trees and more carbon in sapwood.

4 | Discussion

The integration of environmentally-responsive modelled wood density into policy-relevant DGVMs is crucial for accurate estimations of forest carbon sinks. This study explored an approach to model annual mean tree ring density of larch, focusing on earlywood and latewood properties influenced by temperature variables. At the four study sites along a temperature gradient in the Lötschental, the model only reproduced little inter-annual variation of mean tree ring density. This raises important questions about additional factors influencing wood density beyond temperature.

Overall, it is acknowledged that tree rings record environmental conditions in ring width and density, but it is also recognised that a significant amount of variance is non-temperature (non-climate) dependent (Esper et al., 2005, von Storch et al., 2004), which makes modelling based on

environmental conditions more difficult. Uncertainty in the model is likely introduced through the emerging phenology which is dependent on the growing season start (GSS) and LW density. Cuny et al. (2019) demonstrated that trees possess the capacity to adapt to less favourable environmental conditions by exhibiting higher growth rates to compensate for shorter growing seasons. This would mean that GSS is not as important for the width of EW as this model suggests. Instead, other factors such as water availability could be used to model the width of EW. An influence of water availability on EW properties in particular was shown for example by Camarero et al. (2017) and Bytebier et al. (Bytebier et al., 2022). Eckes-Shephard et al. (2021) also proposed a soil water potential response function which was able to reproduce over 60% of observed tree ring width in larch suggesting that the here presented dynamic wood density model would benefit from a soil water dependence. Esper et al. (2015) further demonstrated that tree ring width series exhibit carry-on effects, whereby width is not only dependent on the current year's conditions but also on those of previous years, an effect that is not considered in this model for simulating EW and LW width. The hypothesis put forth by Friend et al. (2022) regarding the dependence of earlywood on carbon availability, implies an additional dependence. Given the multitude of factors influencing wood formation and, consequently, tree ring density, it is challenging to develop a simple model that can adequately explain inter-annual variability in mean tree ring density. The first research question of this thesis should therefore be asked and investigated again considering different approaches to modelling tree ring phenology.

Despite these challenges, the integration of the dynamic wood density model into LPJ-GUESS demonstrated significant effects on tree productivity, carbon content and tree phenology, emphasising the necessity for models to simulate wood density trends. The integration of dynamic wood density into DGVMs affects long-term estimates of carbon storage, which is of great relevance for climate change projections and mitigation strategies (Friend et al., 2014). While the absolute results derived in this thesis have no meaning due to the insufficient validation of modelled mean tree ring density, they highlight the importance of having a validated wood density model as it is shown that it will impact the carbon pools in trees. Carbon stored in leaves and sapwood is altered which implies an impact on the mean carbon residence time in trees, identified as one of the main uncertainties in carbon storage estimations in DGVMs (Pugh et al., 2020).

The dynamic wood density model requires further refinement but is already an additional capability of LPJ-GUESS to incorporate temperature as a limiting factor to stem growth. This model additionally opens future research opportunities including the calibration of the functions for more species and investigating the effect of dynamic wood density on tree mortality and competition in ecosystem models. With an improved wood density model, the contribution of wood density to the minimisation of carbon estimation error can be investigated.

References

Ackerly, D. (2003). Community assembly, niche conservatism, and adaptive evolution in changing environments. *International Journal of Plant Sciences*, (S3), 165–184. https://doi.org/https://doi.org/10.1086/368401

Anderegg, W. R., Klein, T., Bartlett, M., Sack, L., Pellegrini, A. F., Choat, B., & Jansen, S. (2016). Meta-analysis reveals that hydraulic traits explain cross-species patterns of drought-induced tree mortality across the globe. *Proceedings of the National Academy of Sciences of the United States of America*, *113*(18), 5024–5029. https://doi.org/10.1073/pnas.1525678113

Begum, S., Nakaba, S., Yamagishi, Y., Oribe, Y., & Funada, R. (2013). Regulation of cambial activity in relation to environmental conditions: Understanding the role of temperature in wood formation of trees. *Physiologia plantarum*, *147*(1), 46–54. https://doi.org/https://doi.org/10.1111/j.1399-3054.2012.01663.x

Boakye, E., Mvolo, C., & Stewart, J. (2023). Systematic review: Climate and non-climate factors influencing wood density in the boreal zone. *BioResources*, *18*(4). https://doi.org/10.15376/biores.18.4.Boakye

Bytebier, J., De Mil, T., Vanhellemont, M., Verheyen, K., Haneca, K., & Van den Bulcke, J. (2022). Linking wood density records of common beech (fagus sylvatica l.) with temperature and precipitation variability from a temperate lowland site. *Dendrochronologia*, *76*. https://doi.org/https://doi.org/10.1016/j.dendro.2022.126018

Camarero, J., Fernández-Pérez, L., Kirdyanov, A., Shestakova, T., Knorre, A., Kukarskih, V., & Voltas, J. (2017). Minimum wood density of conifers portrays changes in early season precipitation at dry and cold eurasian regions. *Trees*, *31*, 1423–1437. https://doi.org/https://doi.org/10.1007/s00468-017-1559-x

Catesson, A.-M. (1994). Cambial ultrastructure and biochemistry: Changes in relation to vascular tissue differentiation and the seasonal cycle. *International Journal of Plant Sciences*, *155*(3), 251–261. https://doi.org/doi:10.1086/297165

Chao, K.-J., Phillips, O. L., Gloor, E., Monteagudo, A., Torres-Lezama, A., & Martínez, R. V. (2008). Growth and wood density predict tree mortality in amazon forests. *Journal of Ecology*, *96*(2), 281–292. https://doi.org/10.1111/j.1365-2745.2007.01343.x

Chave, J., Coomes, D., Jansen, S., Lewis, S., Swenson, N., & Zanne, A. (2009). Towards a worldwide wood economics spectrum. *Ecology Letters*, *12*(4), 351–366. https://doi.org/https://doi.org/10.1111/j.1461-0248.2009.01285.x

Chave, J., Davies, S. J., Phillips, O. L., Lewis, S. L., Sist, P., Schepaschenko, D., Armston, J., Baker, T. R., Coomes, D., Disney, M., Duncanson, L., Hérault, B., Labrière, N., Meyer, V., Réjou-Méchain, M., Scipal, K., & Saatchi, S. (2019). Ground data are essential

for biomass remote sensing missions. *Surveys in Geophysics*, *40*(4), 863–880. https://doi.org/10.1007/s10712-019-09528-w

Cuny, H., Fonti, P., Rathgeber, C., von Arx, G., Peters, R., & Frank, D. (2019). Couplings in cell differentiation kinetics mitigate air temperature influence on conifer wood anatomy. *Plant, Cell & Environment*, *42*(4), 1222–1232. https://doi.org/https://doi.org/10.1111/pce.13464

Cuny, H., Rathgeber, C., Frank, D., Fonti, P., & Fournier, M. (2014). Kinetics of tracheid development explain conifer tree-ring structure. *New Phytologist*, *203*(4), 1231–1241. https://doi.org/https://doi.org/10.1111/nph.12871

Cuny, H., & Rathgeber, C. (2016). Xylogenesis: Coniferous trees of temperate forests are listening to the climate tale during the growing season but only remember the last words! *Plant physiology*, *171*(1), 306–317. https://doi.org/https://doi.org/10.1104/pp.16.00037

Drew, D., & Downes, G. (2015). A model of stem growth and wood formation in pinus radiata. *Trees*, *29*, 1395–1413.

Düthorn, E., Schneider, L., Günther, B., Gläser, S., & Esper, J. (2016). Ecological and climatological signals in tree-ring width and density chronologies along a latitudinal boreal transect. *Scandinavian Journal of Forest Research*, *31*(8), 750–757. https://doi.org/10.1080/02827581.2016.1181201

Eckes-Shephard, A. H., Ljungqvist, F. C., Drew, D. M., Rathgeber, C. B. K., & Friend, A. D. (2022). Wood formation modeling - a research review and future perspectives. *Frontiers in plant science*, *13*. https://doi.org/https://doi.org/10.3389/fpls.2022.837648

Eckes-Shephard, A. H., Tiavlovsky, E., Chen, Y., Fonti, P., & Friend, A. D. (2021). Direct response of tree growth to soil water and its implications for terrestrial carbon cycle modelling. *Global Change Biology*, *27*(1), 121–135. https://doi.org/https://doi.org/10.1111/gcb.15397

Esper, J., Frank, D. F., Wilson, R. J. S., & Briffa, K. R. (2005). Effect of scaling and regression on reconstructed temperature amplitude for the past millennium. *Geophysical Research Letters*, *32*(5). https://doi.org/https://doi.org/10.1029/2004GL021236

Esper, J., Schneider, L., Smerdon, J. E., Schöne, B. R., & Büntgen, U. (2015). Signals and memory in tree-ring width and density data. *Dendrochronologia*, *35*, 62–70. https://doi.org/https://doi.org/10.1016/j.dendro.2015.07.001

Franceschini, T., Longuetaud, F., Bontemps, J., Bouriaud, O., Caritey, B., & Leban, J. (2013). Effect of ring width, cambial age, and climatic variables on the within-ring wood density profile of norway spruce picea abies (l.) karst. *Trees*, *27*(4), 913–925. https://doi.org/10.1007/s00468-013-0844-6

Friedlingstein, P., O'sullivan, M., Jones, M. W., Andrew, R. M., Gregor, L., Hauck, J., Le Quéré, C., Luijkx, I. T., Olsen, A., Peters, G. P., Peters, W., Pongratz, J., Schwingshackl, C., Sitch, S., Canadell, J. G., Ciais, P., Jackson, R. B., Alin, S. R., Alkama, R., … Zheng, B.

(2022). Global carbon budget 2022. *Earth System Science Data*, *14*(11), 4811–4900. https://doi.org/10.5194/essd-14-4811-2022

Friend, A., Eckes-Shephard, A., & Tupker, Q. (2022). Wood structure explained by complex spatial source-sink interactions. *Nature Communications*, *13*(7824). https://doi.org/https://doi.org/10.1038/s41467-022-35451-7

Friend, A. D., Lucht, W., Rademacher, T. T., Keribin, R., Betts, R., Cadule, P., Ciais, P., Clark, D. B., Dankers, R., Falloon, P. D., Ito, A., Kahana, R., Kleidon, A., Lomas, M. R., Nishina, K., Ostberg, S., Pavlick, R., Peylin, P., Schaphoff, S., … Woodward, F. I. (2014). Carbon residence time dominates uncertainty in terrestrial vegetation responses to future climate and atmospheric co2. *Proceedings of the National Academy of Sciences of the United States of America*, *111*(9), 3280–3285. https://doi.org/10.1073/pnas.1222477110

Fritts, H. (1976). Chapter 1 - dendrochronology and dendroclimatology. In H. Fritts (Ed.), *Tree rings and climate* (pp. 1–54). Academic Press. https://doi.org/https://doi.org/10.1016/B978-0-12-268450-0.50006-9

Funada, R. (2008). Microtubules and the control of wood formation. In P. Nick (Ed.), *Plant microtubules: Development and flexibility* (pp. 83–119). Springer Berlin Heidelberg. https://doi.org/10.1007/7089_2008_163

Funada, R., Yamagishi, Y., Begum, S., Kudo, K., Nabeshima, E., Nugroho, W. D., Hasnat, R., Oribe, Y., & Nakaba, S. (2016). Chapter 2 - xylogenesis in trees: From cambial cell division to cell death. In Y. S. Kim, R. Funada, & A. P. Singh (Eds.), *Secondary xylem biology* (pp. 25–43). Academic Press. https://doi.org/https://doi.org/10.1016/B978-0-12-802185-9.00002-4

Gričar, J., Zupančič, M., Čufar, K., Koch, G., Schmitt, U., & Oven, P. (2006). Effect of local heating and cooling on cambial activity and cell differentiation in the stem of norway spruce (picea abies). *Annals of botany*, *97*(6), 943–951. https://doi.org/https://doi.org/10.1093/aob/mcl050

Gros-Louis, M.-C., Bousquet, J., Pâques, L. E., & Isabel, N. (2005). Species-diagnostic markers in larix spp. based on rapds and nuclear, cpdna, and mtdna gene sequences, and their phylogenetic implications. *Tree Genetics and Genomes*, *1*(2), 50–63. https://doi.org/10.1007/s11295-005-0007-z

Harris, N. L., Gibbs, D. A., Baccini, A., Birdsey, R. A., de Bruin, S., Farina, M., Fatoyinbo, L., Hansen, M. C., Herold, M., Houghton, R. A., Potapov, P. V., Suarez, D. R., Roman-Cuesta, R. M., Saatchi, S. S., Slay, C. M., Turubanova, S. A., & Tyukavina, A. (2021). Global maps of twenty-first century forest carbon fluxes. *Nature Climate Change*, *11*(3), 234–240. https://doi.org/10.1038/s41558-020-00976-6

IPCC. (2019). *Ipcc special report on climate change, desertification, land degradation, sustainable land management, food security, and greenhouse gas fluxes in terrestrial ecosystems*

(P. Shukla, J. Skea, E. C. Buendia, V. Masson-Delmotte, H. O. Pörtner, D. C. Roberts, P. Zhai, R. Slade, S. Connors, R. van Diemen, M. Ferrat, E. Haughey, S. Luz, S. Neogi, M. Pathak, J. Petzold, J. P. Pereira, P. Vyas, E. Huntley, ... J. Malley, Eds.).

Levanič, T., Gričar, J., Gagen, M., Jalkanen, R., Loader, N. J., McCarroll, D., Oven, P., & Robertson, I. (2009). The climate sensitivity of norway spruce [picea abies (l.) karst.] in the southeastern european alps. *Trees*, *23*, 169–180. https://doi.org/https://doi.org/10.1007/s00468-008-0265-0

Matras, J., & Pâques, L. (2003). Euforgen technical guidelines for genetic conservation and use for european larch ((larix decidua)). Retrieved April 29, 2024, from https://www.euforgen.org/species/larix-decidua/

Mo, L., Crowther, T., & et al., D. M. (2024). Consistent climatic controls of global wood density among angiosperms and gymnosperms. *PREPRINT (Version 1)*. https://doi.org/https://doi.org/10.21203/rs.3.rs-3934396/v1

Oribe, Y., & Kubo, T. (1997). Effect of heat on cambial reactivation during winter dormancy in evergreen and deciduous conifers. *Tree physiology*, *17*(2), 81–87. https://doi.org/https://doi.org/10.1093/treephys/17.2.81

Oribe, Y., Funada, R., Shibagaki, M., & Kubo, T. (2001). Cambial reactivation in locally heated stems of the evergreen conifer abies sachalinensis (schmidt) masters. *Planta*, *212*(5/6), 684–691. Retrieved May 1, 2024, from http://www.jstor.org/stable/23386161

Pan, Y., Birdsey, R. A., Fang, J., Houghton, R., Kauppi, P. E., Kurz, W. A., Phillips, O. L., Shvidenko, A., Lewis, S. L., Canadell, J. G., Ciais, P., Jackson, R. B., Pacala, S. W., McGuire, A. D., Piao, S., Rautiainen, A., Sitch, S., & Hayes, D. (2011). A large and persistent carbon sink in the world's forests. *Science*, *333*(6045), 988–993. https://doi.org/10.1126/science.1201609

Pretzsch, H., Biber, P., Schütze, G., Kemmerer, J., & Uhl, E. (2018). Wood density reduced while wood volume growth accelerated in central european forests since 1870. *Forest Ecology and Management*, *429*, 589–616. https://doi.org/https://doi.org/10.1016/j.foreco.2018.07.045

Pugh, T. A. M., Rademacher, T., Shafer, S. L., Steinkamp, J., Barichivich, J., Beckage, B., Haverd, V., Harper, A., Heinke, J., Nishina, K., Rammig, A., Sato, H., Arneth, A., Hantson, S., Hickler, T., Kautz, M., Quesada, B., Smith, B., & Thonicke, K. (2020). Understanding the uncertainty in global forest carbon turnover. *Biogeosciences*, *17*(15), 3961–3989. https://doi.org/10.5194/bg-17-3961-2020

Rosell, J., Olson, M., & Anfodillo, T. (2017). Scaling of xylem vessel diameter with plant size: Causes, predictions, and outstanding questions. *Currrent Forestry Reports*, *3*, 46–59. https://doi.org/https://doi.org/10.1007/s40725-017-0049-0

Semerikov, V. L., & Lascoux, M. (1999). Genetic relationship among eurasian and american larix species based on allozymes. *Heredity*, *83*(1), 62–70. https://doi.org/10.1038/sj.hdy.6885310

Vaganov, E. A., Hughes, M. K., & Shashkin, A. V. (2006). *Growth dynamics of conifer tree rings: Images of past and future environments*. Springer Verlag.

van der Maaten, E., van der Maaten-Theunissen, M., & Spiecker, H. (2012). Temporally resolved intra-annual wood density variations in european beech (fagus sylvatica l.) as affected by climate and aspect. *Annaly of forest research*, *55*(1). https://doi.org/https://doi.org/10.15287/afr.2012.83

von Storch, H., Zorita, E., Jones, J. M., Dimitriev, Y., González-Rouco, F., & Tett, S. F. B. (2004). Reconstructing past climate from noisy data. *Science*, *306*(5696), 679–682. https://doi.org/10.1126/science.1096109

Wei, X.-X., & Wang, X.-Q. (2004). Recolonization and radiation in larix (pinaceae): Evidence from nuclear ribosomal dna paralogues. *Molecular Ecology*, *13*(10), 3115–3123. https://doi.org/10.1111/j.1365-294X.2004.02299.x

Wei, X.-X., & Wang, X.-Q. (2003). Phylogenetic split of larix: Evidence from paternally inherited cpdna trnt-trnf region. *Plant Systematics and Evolution*, *239*(1-2), 67–77. https://doi.org/10.1007/s00606-002-0264-3

Yang, H., Wang, S., Son, R., Lee, H., Benson, V., Zhang, W., Zhang, Y., Zhang, Y., Kattge, J., Boenisch, G., Schepaschenko, D., Karaszewski, Z., Stereńczak, K., Moreno-Martínez, Á., Nabais, C., Birnbaum, P., Vieilledent, G., Weber, U., & Carvalhais, N. (2024). Global patterns of tree wood density. *Global Change Biology*, *30*(3), e17224. https://doi.org/https://doi.org/10.1111/gcb.17224

Appendix A: Paper Draft

Including environmental-depending wood density in vegetation models

Anna-Kristina Voss[1], Stefan Olin[1], Hao Zhou[1], Patrick Fonti[2], Annemarie H. Eckes-Shephard[1]

[1] Department of Physical Geography and Ecosystem Science, Lund University, Lund, Sweden

[2] Swiss Federal Institute for Forest, Snow and Landscape Research WSL, Birmensdorf, Switzerland

Abstract

Wood density is a crucial trait in trees influencing carbon storage in forests, yet dynamic global vegetation models (DGVMs) neglect its variability under different environmental conditions. In this study, we integrate environmentally-dependent wood density into the DGVM LPJ-GUESS by simulating mean annual tree ring density based on temperature variables. The model considers earlywood and latewood as crucial structural parts in temperate tree rings, deriving mean tree ring density from the width and density of these components. Validation at sites along a hill slope in Lötschental, Switzerland on European larch (Larix decidua), showed that while the model captured mean wood density trends across elevations, it did not reproduce annual mean tree ring density. We compared the versions of LPJ-GUESS, with and without dynamic wood density. Results indicate that dynamic wood density impacts trees' annual net primary productivity (ANPP) and carbon storage in leaves and sapwood. However, these changes could not be consistently associated with increases in wood density relative to the wood density parameter of LPJ-GUESS without dynamic wood density, suggesting complex effects on tree allocation dynamics. Average tree height per age group was consistently lower in LPJ-GUESS-WD across elevations, regardless of ANPP variations, with a negative correlation observed between mean height difference and stem density. These findings underscore the importance of incorporating dynamic wood density in DGVMs due to its impact on predictions of forest carbon dynamics and tree growth patterns.

Introduction

Forests are crucial in regulating Earth's climate by acting as a significant carbon sink to anthropogenic emissions. A central aspect to carbon storage is the investment of trees in woody biomass, wherein over 50% of a tree's carbon is stored (Pan et al., 2011, Mo et al., 2024). The density of formed wood determines how much carbon is stored in wood and it also serves multiple physiological purposes which make it a crucial functional trait. Wood density emerges through the wood formation process and influences various ecological functions including mechanical support, nutrient storage, and water transport (Ackerly, 2003, Chave et al., 2009, Ogle et al., 2014, Cuny et al., 2019). Furthermore, it impacts biomass ratios between the tree compartments (Mencuccini et al., 2019). As an adaptive trait, wood density exhibits considerable variability influenced by factors such as species, climate, and ecosystem type (Mo et al., 2024). In temperate zones, wood formation occurs in annual growth cycles, resulting in distinct tree rings composed of earlywood and latewood (Cuny et al., 2014). Environmental factors, including temperature and water availability, influence the inter- and intra-annual variability of density (Rosell et al., 2017, Buttò et al., 2020, Camarero and Hevia, 2020, Begum et al., 2018). Research on the impacts and controls of wood density has significantly advanced, yet this progress is not reflected in the mechanisms of major ecosystem models (Micco et al., 2019). Global dynamic vegetation models (DGVMs), commonly do not represent wood density emerging from environmental conditions trees are exposed to instead treating it as a species or plant functional type specific parameter. This may have implications on predicting ecosystem carbon content itself, but also the dynamics of ecosystem responses to climate change (Mo et al., 2024, Yang et al., 2024).

Temperate tree rings follow a common pattern of density, gradually increasing from low densities to significantly higher densities (Fig. 1). Depending on species, the maximum density is reached at the end of the ring or slightly earlier followed by a slight decrease in density at the end of the ring (Fritts, 1976). The less-dense earlywood (EW) is characterised by larger, thin-walled cells resulting from its formation being dominated by cell enlargement rather than wall-thickening at the beginning of the growth season. The latewood (LW) is denser and consists commonly of narrow, thick-walled cells due to secondary wall-thickening dominating its formation in the later growing season (Cuny et al., 2014). When wanting to derive mean annual wood density useful for a vegetation model, one therefore needs to consider both the EW and LW density and their fraction in the tree ring (Fig. 1). All these variables are both dependent on environmental and tree-internal processes.

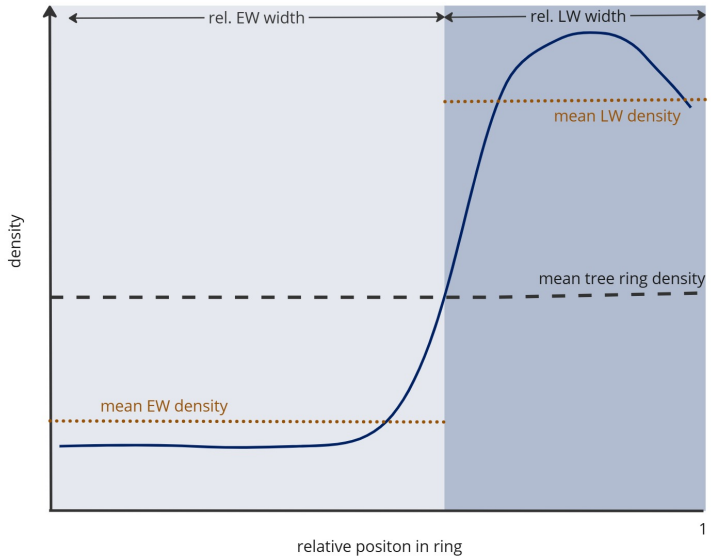

Figure 1: Illustration of a default density profile in a temperate tree ring consisting of earlywood (EW, light) and latewood (LW, dark) with the modelled properties

Studies have shown that EW density positively correlates with early season temperatures and correlates negatively with spring precipitation (Camarero and Hevia, 2020, Camarero et al., 2017, Bytebier et al., 2022). Overall, the results on environmental controls of EW properties, both width and density, are inconclusive. One possible reason for this are compensatory effects between rates and durations during the formation (Cuny et al., 2019, Cuny and Rathgeber, 2016). Friend et al. (2022) further proposed that limited carbon availability in the early season could restrict EW density. Positive correlations between tree ring LW density and maximum density with late summer temperatures, have been consistently reported, indicating an effect of temperature on LW formation (Boakye et al., 2023, Cuny et al., 2019, van der Maaten et al., 2012, Düthorn et al., 2016, Levanič et al., 2009). Pritzkow et al.,(2014) also reports a correlation of summer temperatures with total ring density.

Tree ring records are frequently used to reconstruct past climate, and tree ring width and maximum density have been prominent variables for the reconstruction of precipitation and temperature and temperature respectively (Beeckman, 2016). Tree ring width is dominated by EW width, making up on average 70% of the annual tree ring (Düthorn et al., 2016, Cuny et al., 2014). In areas without water limitation, the onset of growing season has therefore been suggested to be the driver for EW width (Cuny et al., 2019, Pretzsch et al., 2018). The stem growing season starts with the reactivation of cell division in the cambium which is controlled by temperature (Oribe and Kubo, 1997, Oribe et al., 2001, Gričar et al., 2006, Begum et al., 2013). Cuny et al. (2019) showed in the Swiss Alps that linear dependence of the cell divison starts in spring after dormancy on annual mean temperatures. The transition from EW to LW has previously been studied, but its controls have yet to be determined with certainty (Eckes-

Shephard et al., 2022), but some research suggests that the transition from EW to LW may be site-dependent based on photoperiod (Wang et al., 2023, Gričar et al., 2021, Rathgeber, 2017). As a consequence of a more or less fixed transition date determined by latitude, an earlier or later onset of the growing season could shift the ratio between EW and LW formation (Pretzsch et al., 2018, Lupi et al., 2010).

The complexity of the emergence of wood density and the wood formation process in general make it hard to model. One model reported by Franceschini et al. (2013) uses the common pattern of EW, transition wood and LW in tree rings. For each of these three wood types, the model determines the onset of formation as the relative position in the ring, an initial density, and a slope representing the increase in density in the wood type. All values increase from EW over transition wood to LW. The model is complex due to many variables and has many different inputs such as temperature, precipitation, or vapour pressure deficit.

We developed a dynamic wood density model based on 1) a temperature-dependent LW density function and 2) a phenology function. We investigated different versions of these functions and their contribution to the ability of the model to replicate the general behaviour of wood density in European Larch across an elevational transect in the Swiss Alps. European larch (*Larix decidua*), prevalent in the Swiss Alps where this research is focused, primarily inhabits mountainous regions and spans approximately 500,000 hectares with a fragmented distribution (Matras and Pâques, 2003). Larch was chosen as a species here due to the abundant availability of data for both function construction and the model validation. We verify the extent to which the dynamic wood density model can replicate elevation-dependent and thereby temperature-driven variability, and distinct climate-induced trends based on four validation sites along a hillslope in Lötschental, Switzerland. Our hypothesis is that the phenology function will contribute to a better model performance compared to default phenology.

We integrated the dynamic wood density model into the DGVM LPJ-GUESS, one of the state of the art vegetation models (Smith et al., 2014). Until now, the plant functional type specific parameter values in LPJ-GUESS failed to represent the variability of wood density under environmental variations. In LPJ-GUESS with the integrated wood density model (hereafter LPJ-GUESS-WD), dynamic wood density will affect carbon allocation and tree growth. We compared outputs of LPJ-GUESS-WD against the static wood density implemented in the standard LPJ-GUESS. We analysed the effect of dynamic wood density in LPJ-GUESS on tree growth of European Larch exemplary at three different elevations in Lötschental. This research aims to address the inherent limitation of the non-variable wood density in LPJ-GUESS by replacing it with a dynamic wood density based on the functions presented. The aim of the study is to create a model that replicates wood density's response to climatic variations and allows for environmental-dependent inter-annual variability in wood density that influences the growth

processes in LPJ-GUESS.

Methods and Data

Modelling dynamic wood density

The dynamic wood density model consists of two elements 1, the latewood density function and 2, the phenology function. The latewood density function returns the average LW density based on summer temperatures. Phenology is modelled with two functions returning the EW width and LW width respectively. The results of these three functions are used alongside an EW density parameter to determine the annual mean tree ring density. The model is inspired by the basic concept of the model reported by Franceschini et al. (2013). Annual tree ring average density (TRD) is calculated as

$$TRD = \frac{EWW \cdot EWD + LWW \cdot LWD}{EWW + LWW} \tag{1}$$

where EWW and LWW are earlywood and latewood width respectively and EWD and LWD are the earlywood and latewood density respectively.

Latewood density function

The latewood density function returns a modification factor that modulates LW density relative to the species-specific EW density parameter. The modification factor (hereafter LW-factor) is dependent on average July-August temperatures. July and August were used as they were the single months with the highest correlation (R^2 = 0.23 and R^2 = 0.21) between temperature and LW-factor and the average temperature across July and August was the period with the highest correlation overall (R^2 = 0.33) (for all tested temperature variables, see Fig. B2). The temperature-response function was built on binned, observed data. We tested several functions and selected the best fitted logistic growth function, as it conforms with the hypothesis of relative stability of LW density outside of the range of observed temperature values (Fig. 2a). For detailed information on function construction and binning refer to Appendix B: Supplementary Material on Methods and Data (p. B-1).

For testing our first hypothesis, the simple model with only dynamic LW density assumed a 70% share of EW of the tree ring width and 30% respectively being LW. This was the mean relationship obtained from initial analysis of the observational data for function construction (Fig. B5). The EW density was set to the mean observed EW density in European larch at 167 kgC/m^3 (Appendix B: Binning and function building, p. B-14).

Phenology function

The phenology within a tree ring partitioning it into EW and LW is determining the contribution of EW and LW density to the annual mean tree ring density. Studies have found that growing season length is a factor in determining tree ring width and especially EW width (Lupi et al., 2010, Rossi et al., 2014, He et al., 2018, Pretzsch et al., 2018). Our analysis of observational data has further found a relationship between growing season start (GSS) and EW width. The observational data for function construction also shows a non-linear relationship between LW density and LW width. Thus, we constructed two functions that 1) consider growing season onset and 2) LW density and thereby projects how much of the total tree ring width is made up by EW and LW respectively.

We assumed that the growing season is an important factor driving variations in ring composition with an early beginning of the growing season for wood causing wider EW to be formed. This was previously suggested by Pretzsch et al. (2018). The GSS was calculated based on the annual average temperature as proposed by Cuny et al. (2019). The data was binned per unique GSS date, assuming the same GSS leads to similar EW widths. The bins showed a linear trend to which a linear function was fitted with the lm-function in R (Fig. 2b). For more information refer to Appendix B: Supplementary Material on Methods and Data (p. B-1).

LW width showed an exponential relation to LW density in the observations on which the LW width function is based. Binned average LW density was plotted against binned average LW width and an exponential growth function was fitted using the nls-function in R (Fig. 2c). All three functions and an EW density as for the simpel model of 167 kgC/m^3 (Appendix B: Binning and function building, p. B-14) contribute to modelling mean tree ring density.

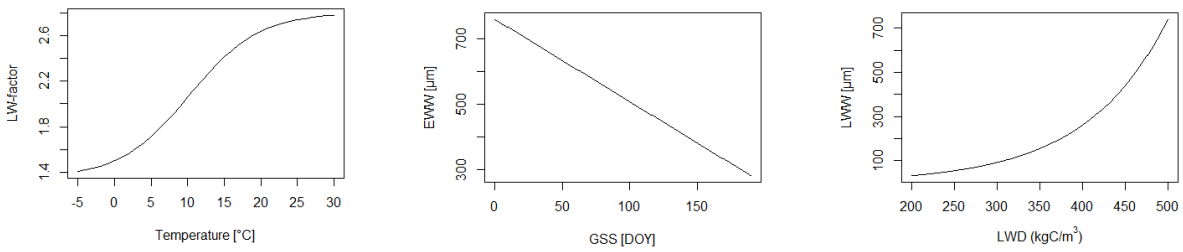

(a) $1.35 + \frac{2.8-1.35}{1+e^{(-0.21\cdot(T-10.2))}}$ **(b)** $758.41 - 2.51 \cdot GSS$ **(c)** $4.0832 \cdot e^{0.0104 \cdot LWD}$

Figure 2: Functions forming the tree ring density model consisting of (a) a function modelling a latewood factor (LW-factor) modifying earlywood density to obtain latewood density based on the mean July-August temperature, (b) a function modelling earlywood width based on the growing season start given as day of the year (DOY) and (c) a function modelling latewood width in depending on latewood density.

Observational data

Model building

For function building, we used observed data from the International Tree Ring Database (ITRDB) (National Oceanic and Atmospheric Administration (NOAA), 2022) which we selected to be larch growing in Europe or Russia. Datasets needed to have EW and LW density and width as reported variables. The data stem from 84 sites, mainly in Russia with one in Switzerland, including European larch (*Larix decidua*), Dahurian larch (*Larix gmelinii*) and Siberian larch (*Larix sibirica*) (List of all sites in Tab. B1).

Original width data was first detrended with the dplR package (Vers. 1.7.4) in R based on total tree ring widths and EW and LW width were multiplied with the returned tree ring width index. Density values were given in kg/dry mass and were transformed into kgC/m^3 by multiplying with the average share of carbon in biomass of 0.5.

All data were averaged per year and site for the years 1901 to 1999. Outliers were removed based on their z-score so that values with a z-score greater than 3 were discarded (Appendix B, Eq. B1). The climate data used for both the LW density function construction and for calculating the stem growing season start are CRU JRA data (University of East Anglia Climatic Research Unit, 2020) available as mean gridded data with grid sizes of 0.5 °. Because CRU JRA provides mean temperatures at the mean elevation of a grid cell, the temperature values were modified based on the elevation of the sites and the reference elevation for the climate data. A lapse rate of 0.649°C/100m was used for the modification matching the one used in LPJ-GUESS.

We used binning to fit the LW density function and functions for the phenology. Binning is performed to account for variability in the variables (LW density, EW width, LW width) that are unrelated to the respective independent variable (Eckes-Shephard et al., 2021). Further, the data was biased with the majority of the data in just a small fraction of the total range of the independent variable (Appendix B: B2). With a one-way analysis of variance, it was confirmed that the average value of each bin was significantly differing from the other bins.

Validation data

We compared the dynamic wood density model output against observational data, before integrating it into LPJ-GUESS. The model was run on CRU JRA data (University of East Anglia Climatic Research Unit, 2020) treated as described above for the ITRDB data. The validation data is available for a south-facing slope and the valley of the Lötschental, Switzerland (46.40 N, 7.75 E) (Fig. 3). Data are collected along the Lötschental tree growth monitoring transect for a tree growth monitoring project of the Swiss Federal Institute for Forest, Snow and Landscape

Research (WSL). Data are available for four sites with varying water availability at three different elevations from 1300 m to 2200 m a.s.l. (Tab. 1). The data include total ring width, LW width, and min, max and mean relative density for total ring, EW and LW. Relative density is calculated as the cell wall area relative to the total cells area.

Table 1: Validation sites in Lötschental, Switzerland and the respective years of data availability

ID	Elevation	Classification	Years
N13W	1300 m	wet	2002-2015
N13D	1300 m	dry	2008-2015
S19D	1900 m	dry	2004-2015
S22W	2200 m	wet	1901-2015

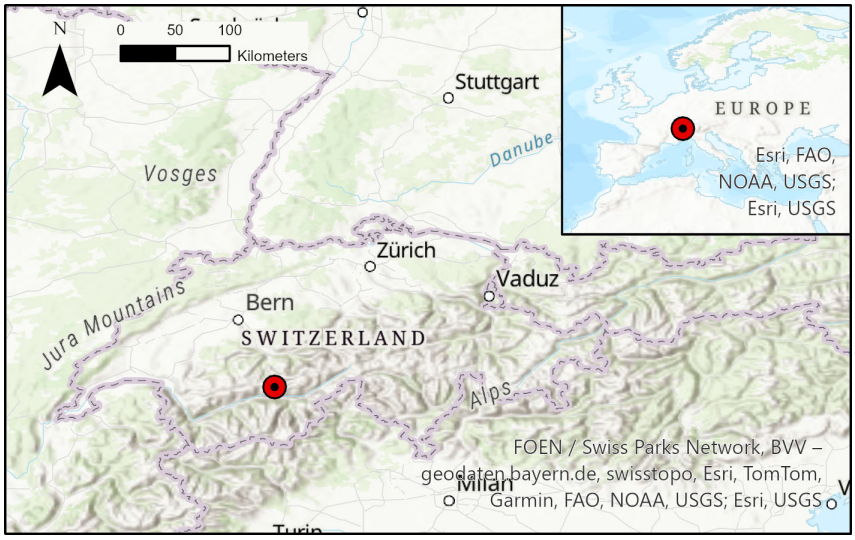

Figure 3: Map showing the location of Lötschental, Switzerland

LPJ-GUESS

The Lund-Potsdam-Jena General Ecosystem Simulator (LPJ-GUESS) (Smith et al., 2001) was the target dynamic global vegetation model (DVGM) for the integration of dynamic wood density into ecosystem models. LPJ-GUESS simulates the emergence of climatically determined vegetation in a grid cell based on meteorological data and soil properties. The vegetation is classified into plant functional types, which are parameterised to possess distinct properties, and strategies to compete for resources. The model operates on daily time steps for the processes of photosynthesis, respiration, phenology, soil nutrient, and carbon cycling and hydrology. Biomass growth allocation, turnover, establishment, and mortality occur annually. In the cohort mode, trees are modelled in age groups with assigned characteristics like diameter, height, or crown area. A trees biomass pool is divided into leaves, roots, sapwood and heartwood. For each grid cell, a predetermined number of stands are established, each consisting of various

patches. Patches are replicate samples within a stand that differ in vegetation composition due to stochastic disturbances such as storms or landslides, which results in vegetation loss within a patch, followed by the reestablishment of vegetation. Establishment resulting from reproduction and mortality is influenced by resource availability and specific requirements and limitations of plant functional types and has a stochastic component. Soil carbon and nitrogen cycling are modelled using the CENTURY model (Parton, 1996). The soil hydrology is simulated with a "leaking-bucket" model for 15 soil layers across the first 1.5 m depth with each layer having a depth of 10 cm. For a more detailed explanation of the basic concepts LPJ-GUESS, refer to Smith et al. (2014).

A topography model has been added into LPJ-GUESS for this study. The model takes into account the elevation, slope, and aspect of a hill slope to simulate stands at different elevation level which are given as inputs together with their respective fraction they cover of the slope. Vegetation is driven by the local climate, which is modified based on the stand's elevation relative to the average grid cell elevation with a lapse rate of 0.649°C/100m. The aspect influences the incoming radiation of a stand, and the slope plays a role in runoff, thereby modifying individual stand's soil moisture available for tree growth.

Integration of the wood density model

The allocation of new biomass determines the distribution of carbon among tree compartments, litter and the turnover from sapwood to heartwood of a plant individual. Two equations are set up in which the increase in height is expressed as an increase in volume (Eq. 2) and an increase in mass (Eq. 3). Wood density is one determinant in the height gain equations for the amount of carbon distributed to the different compartments. The new height (H_n) expressed in volume derives from

$$H_n = \frac{C_S + dBM - dC_L \cdot (1 + \frac{1}{L:R})}{C_L + dC_L} \cdot \frac{K_{LA:SA}}{\overline{\mathbf{WD_t}} \cdot SLA} \tag{2}$$

in which C_S and C_L are the carbon bound in sapwood and in leaves respectively, dBM is the change in biomass and dC_L is the change of carbon in leaves. $L:R$ is the ratio of carbon in leaves to carbon in roots. By that $dBM - dC_L \cdot (1 + \frac{1}{L:R})$ expresses the change in carbon in sapwood. $K_{LA:SA}$ is the leaf area to sapwood area parameter and SLA is the specific leaf area. The default wood density parameter is replaced with $\overline{WD_t}$ which is the total wood density of the stem at the current time t. The new height in mass is calculated as

$$H_n = \frac{C_S + C_H}{\overline{\mathbf{WD_{t-1}}} \cdot \pi \cdot \frac{DBH}{2}^2} + \frac{dBM - dC_L \cdot (1 + \frac{1}{L:R})}{\mathbf{WD_t} \cdot \pi \cdot \frac{DBH}{2}^2 \cdot (\frac{4H}{K_{A2} \cdot K_{A3} \cdot DBH^{K_{A3}}} + 1)} \tag{3}$$

where C_H is the carbon in heartwood and DBH the stem diameter at breast height. $\overline{WD_{t-1}}$ is the total wood density of the stem until the previous year $(t-1)$ and replaces the parameterised wood density. H is the height of the previous year, WD_t is the wood density of the current years tree ring and K_{A2} and K_{A3} are allocation variables dependent on i.e. wood density and $K_{LA:SA}$. The first addend expresses the mass of the tree of the prior year and the second addend expresses the mass gain of the current year. By balancing Eq. 2 and Eq. 3 the leaf carbon increment can be determined. Based on the leaf-to-root (L:R) parameter, the carbon root increment can be calculated. The sapwood increment is the carbon not utilised for leaf and root formation.

Dynamic wood density is only calculated for trees of at least 10 years assuming different growth and allocation patterns in juvenile trees resulting in different densities than the dynamic wood density returns. When trees are old enough, dynamic wood density is updated yearly as shown in Eq. 1 and the resulting tree rings density applied in the total tree trunk density (WD_t) which is updated through

$$\overline{WD_t} = \frac{\frac{C_S+C_H}{dens} \cdot \overline{WD_{t-1}} + dC_s \cdot WD_t}{C_S + C_H + dC_S} \tag{4}$$

with C_S and C_H making up the carbon in wood from the previous year and $dens$ being the density of trees per area.

The allocation scheme is executed twice as the allocation and update of the total trunk density are mutually dependent on each others outcome. The first execution of the allocation happens after the calculation of the current tree rings density (Eq. 1) but assumes the same total trunk density of the previous and current year ($\overline{WD_{t-1}} = \overline{WD_t}$). With the resulting sapwood increment (dC_S) is the total trunk density updated (Eq. 4). The allocation is updated again with the updated total trunk density. If the results for sapwood increment from the two executions differ by more than 25%, the allocation is executed a third time.

Experimental runs

The performance of LPJ-GUESS with an integrated dynamic wood density (LPJ-GUESS-WD) was assessed against the model performance with the standard parameterised wood density (standard LPJ-GUESS) in a spatially and temporally constrained setting. The wood density parameter was set to 220 kgC/m^3 oriented on observed average annual tree ring density values in Switzerland at 1900 m. The value of $K_{LA:SA}$ was adjusted linearly to the change of the wood density parameter for larch. LPJ-GUESS was run for the Lötschental hillslope for three stands with elevations at 1300, 1700 and 2000 m.a.s.l. respectively and a slope of 0 ° and an aspect of 200 ° for all stands. Runs included 5 patch replicates per stand. Only one plant-functional

type, the boreal needleleaved summergreen trees, representing European Larch was included and thereby inter-species competition excluded from the experiment. The experiment was run from 1700 to 2015 using default forcing data until 1900 and for 1901-2015 observed CRU JRA data (University of East Anglia Climatic Research Unit, 2020). All patches across all stands got a clear cut in 1700 and all natural disturbance after was deactivated.

Results

Validation of the dynamic wood density model

The dynamic wood density model was validated for its ability to reproduce trends across elevations and inter-annual variations. For long-term trends, S22W was analysed due to sufficient data availability. The focus was on latewood (LW) density and earlywood (EW) and LW width, followed by total tree ring density. LW density, modelled as a function of July and August temperatures, captured general trends across elevations, with highest density at N13D/W and lowest at S22W. The model explained 57% of inter-annual variations in LW density, with varying performance across sites (R^2 = 0.31 for S22W and N13D) (Fig. 4a). Long-term trends of modelled LW density at S22W showed an upward trend, consistent with observed LW density increase (Fig. 4b). However, the upward trend in in the model was steeper than in the observations (0.02 kgC/m³/yr observed vs. 0.05 kgC/m^3/yr modelled).

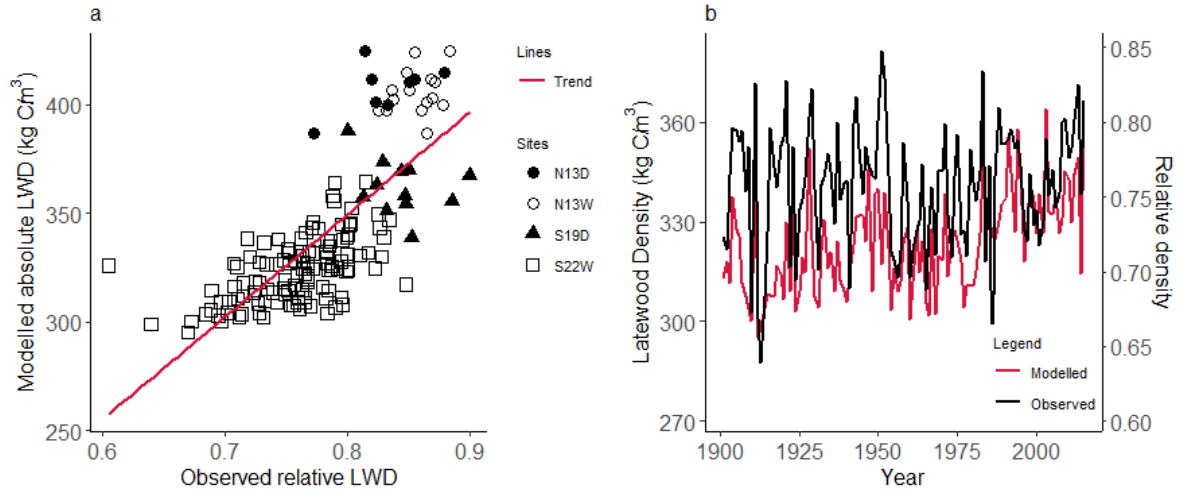

Figure 4: Observed relative mean latewood density and modelled absolute latewood density compared (a) for all sites and (b) only for S22W as time series.

The variability in EW width was reproduced by 32% overall and up to 19% per site (Fig. 4a). LW width variability was explained by 22% across all sites, with a maximum of 24% at one site (S22W) (Fig. 3b). The model underestimated widths of both EW and LW, particularly at lower

elevations. Furthermore, the model shows a strong trend of decreased widths with increased elevation for both EW and LW which is less pronounced in observed data.

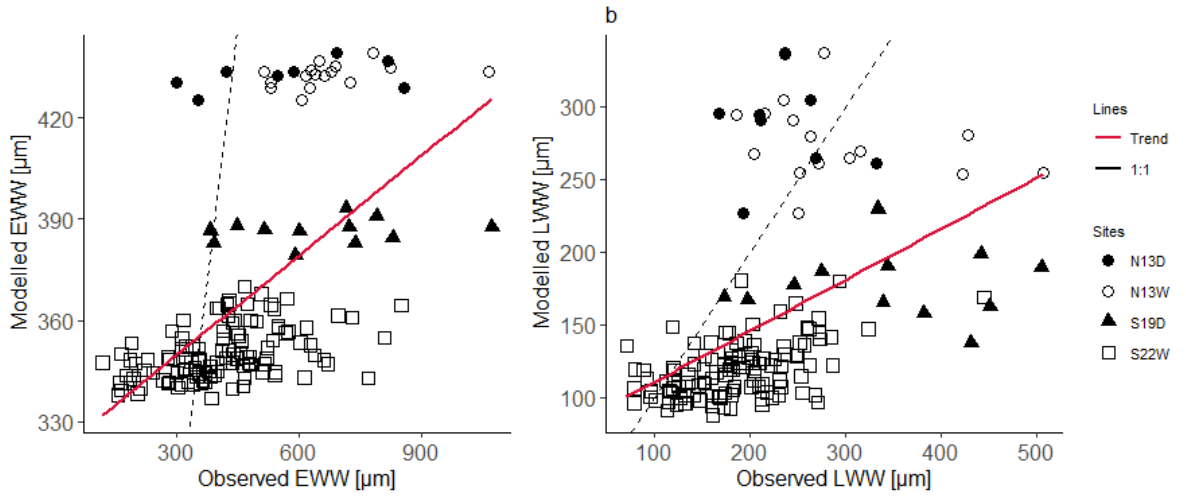

Figure 5: Observed mean earlywood width (EWW, a) and mean latewood width (LWW, b) plotted against the respective modelled widths across the four sites

The model, using a default EW density and a 70:30 EW:LW width ratio, explained 12% of mean annual tree ring density across all sites (Fig. 6a). The maximum inter-annual tree ring density variation reproduced was 11% at S22W and N13D. The semi-mechanistic model explained 12% and 10% of mean annual wood density variability at the two best-performing sites (N13D & S22W), and 11% across all sites (Fig. 6b).

Besides the reproduction of variability, we also compared the across elevation trends. In the observations, relative mean annual tree ring density was 0.49 and relative to that for S19D, N13W, and N13D by 6.1%, 2.0% and 10.0% greater, respectively. The simple model more accurately explained the relative increase in wood density with decreasing elevation, which the phenology model overestimated (Tab. B4). The simples model captured the pattern of increased mean tree ring density with decreasing elevation, with increases in mean density relative to S22W of 5.4%, 11.6%, and 11.7% for S19D, N13W, and N13D, respectively. When modelled phenology is included, the increases in mean density with decreasing altitude was relative to S22W 10.5%, 26.0% and 26.6% for S19D, N13W and N13D respectively (Tab. B5).

Modelled mean ring densities ranged from 200 to 250 kgC/m^3 in the simple model and from 190 to 280 kgC/m^3 when incorporating variable phenology. The percentual range of mean annual tree ring density relative to the mean time series value was represented better with included phenology across all sites. The simple model underestimated the relative range and thereby variability in the mean annual tree ring denities (Tab. B4).

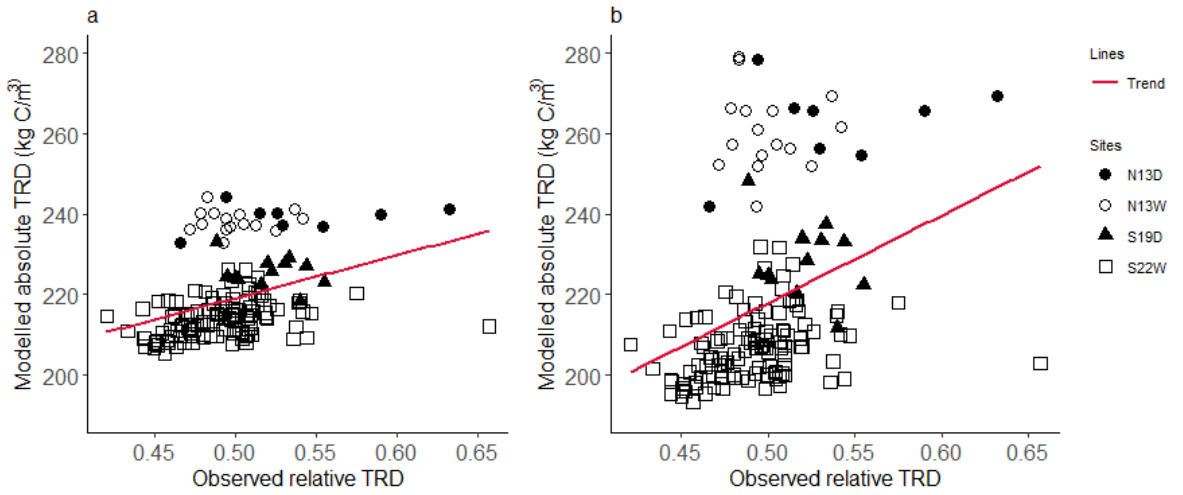

Figure 6: Observed mean tree ring density plotted against the modelled tree ring density across the four sites for (a) the simple model using a default phenology and (b) the model with emerging phenology.

Comparison of LPJ-GUESS-WD to the standard LPJ-GUESS

We simulated larch forests in LPJ-GUESS including environmental-dependent wood density (LPJ-GUESS-WD) and in the standard LPJ-GUESS for a 315-year period following a preset clearcut in 1700 for three stands representing three elevations in the Swiss Alps. The output of the runs were compared with respect to the growth dynamics of trees. The highest stand at 2000 m had only little tree growth over the majority of the time period in both model versions and is therefore largely excluded from further analyses of the results.

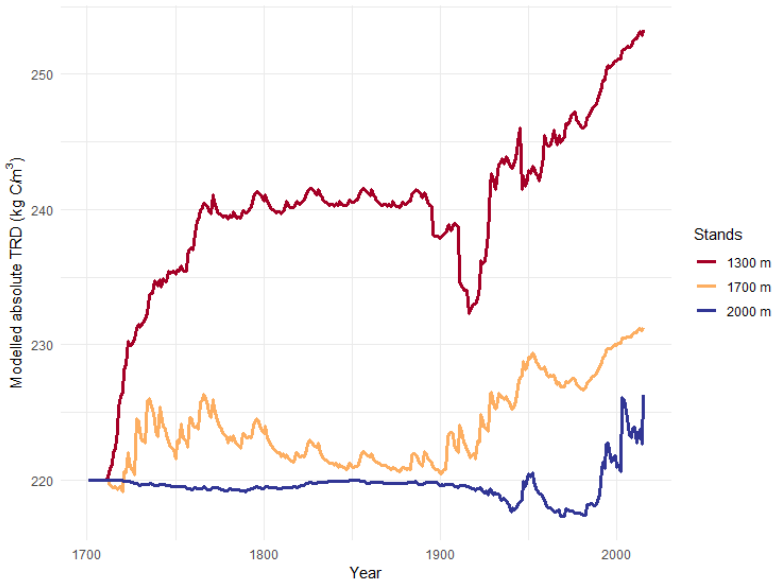

Figure 7: Comparison of modelled mean stem density of trees at three different elevations in Lötschental, Switzerland each modelled in LPJ-GUESS-WD.

LPJ-GUESS-WD simulations showed significant differences in stem densities across elevations (Fig. 7). Wood density was highest at the lowest elevation (1300 m) and lowest at the highest elevation (2000 m), with an increase in wood density at all stands observed from the beginning of the 20^{th} century and onwards.

At low elevation, average annual net primary productivity (ANPP) across the whole time-period was 1.9% lower in LPJ-GUESS-WD than in the standard model, while at mid-elevation, it was 10.8% higher in LPJ-GUESS-WD (Fig. 8a). Carbon mass in leaves was 5.3% lower at low elevation and 10.8% higher at mid-elevation in LPJ-GUESS-WD (Fig. 8c). Sapwood carbon content was increased at both low and mid-elevation in LPJ-GUESS-WD compared to the standard version by 3.3% and 8.2% respectively (Fig. 8d).

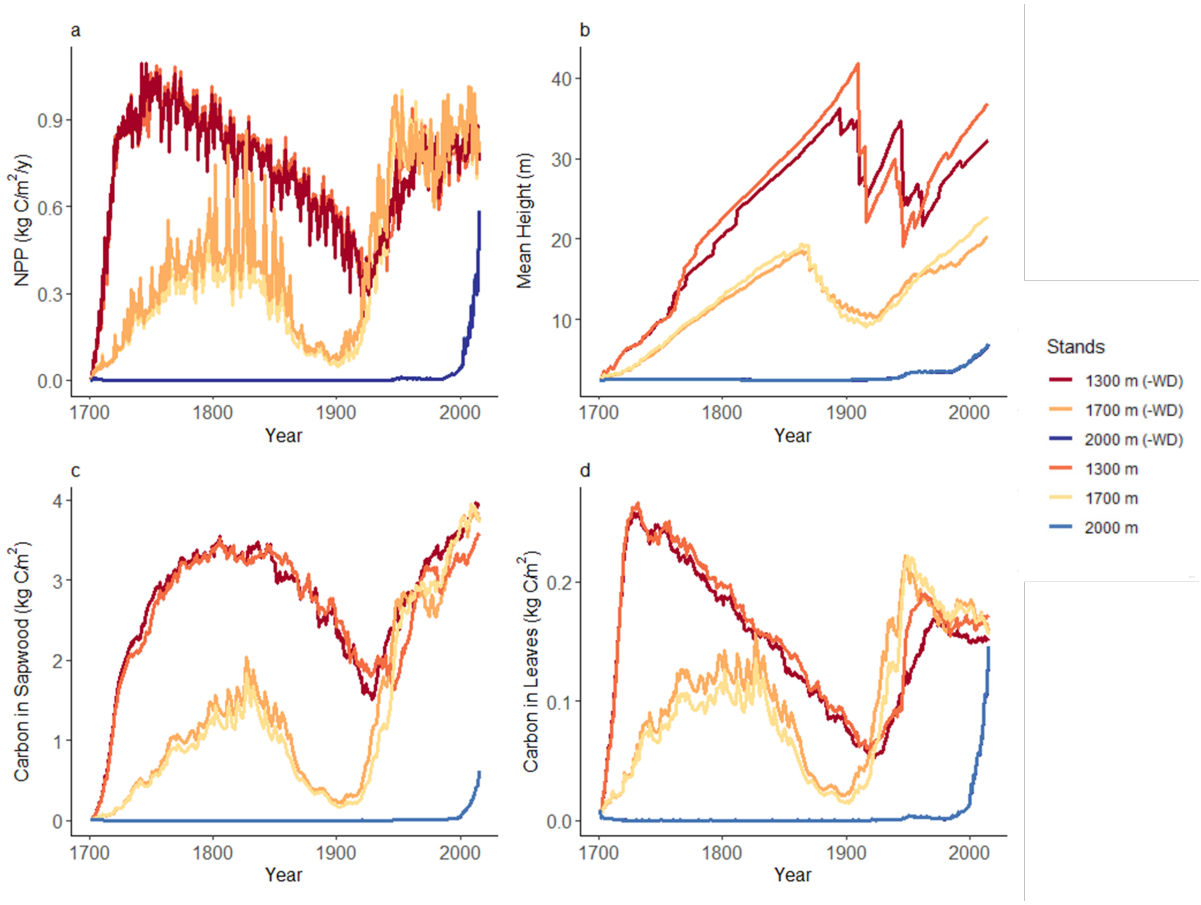

Figure 8: Comparison of (a) modelled annual net primary productivity (ANPP, kgC/m^2/yr), (b) modelled mean height (m), (c) carbon in leaves (kgC/m^2) and (d) carbon in sapwood kgC/m^2 for three stands at different elevations in the Lötschental, Switzerland in the standard LPJ-GUESS and LPJ-GUESS-WD (-WD).

The average tree height was generally higher in the standard model at low and mid-elevations, except between 1900 and 1950 (Fig. 8b). Because that period correlated with a great difference in average age between standard LPJ-GUESS and LPJ-GUESS-WD at both stands, we analysed the average tree height per age group (Tab. 2). For all elevation-age combinations, trees were on

average shorter in LPJ-GUESS-WD than in the standard LPJ-GUESS with a difference of up to 19% at low elevation for 80 year old trees.

Table 2: Average height in age groups of 30, 50 and 80 years of the standard LPJ-GUESS (std.) and LPJ-GUESS-WD (-WD) at three different elevations in Lötschental, Switzerland. For each group, mean height (H_{mean}) is given in meters and wood density (WD) in kgC/m^3.

Age	Version	1300 m		1700 m		2000 m	
		H_{mean}	WD	H_{mean}	WD	H_{mean}	WD
30	std.	7.66	220	6.42	220	2.52	220
	-WD	7.41	233	6.24	225	2.52	220
50	std.	10.19	220	8.94	220	2.61	220
	-WD	9.72	236	8.64	224	2.58	219
80	std.	19.37	220	12.34	220	2.79	220
	-WD	15.65	239	11.79	223	2.70	219

Discussion

Dynamic, mechanistically modelled wood density is currently not part of policy-relevant DGVMs, despite the relevance of wood density for forest carbon sink estimation and vegetation dynamics. We explored an approach to easily implement the environmental dependence of wood density and to model annual mean tree ring density for larch. To do this, we tested a semi-mechanistic approach by considering the two building blocks of tree rings in temperate zones, earlywood and latewood and their width and density as critical properties determining mean tree ring density. We have modelled two of these, EW width and LW density, directly depending on temperature variables and LW width modelled based on LW density, indirectly depending on temperature.

It was possible to reproduce inter-annual variations of the different variables with the model, although the model performance was strongly site dependent. The reasons for the model performing better at some sites could not be explained based on characteristics, and none of the functions performed significantly better or worse at sites classified as dry or wet, or at higher or lower elevations. However, two of the validation sites are known to be different in water availability (N13D & N13W), but are treated the same by LPJ-GUESS-WD due to the same altitude, which is decisive for the temperature variables in the wood density model. Surprisingly to us, N13D was better reproduced by the temperature-dependent model despite being classified as water-limited. To identify the factors that drive better or worse model performance, the model needed to be tested at more sites. As the current model is solely driven based on temperature variables and statistical relationships, including water availability could be a promising approach for improving the model performance such as for the differences between N13D and N13W of the

validation sites. For earlywood width and density, research has indicated that water availability may be an important factor (Camarero et al., 2017, Bytebier et al., 2022) and an approach to model tree ring width in response to water availability was proposed by Eckes-Shephard et al. (2021). While tree ring formation is known to record climate conditions during the tree rings growth, many factors beyond impact a tree rings formation which are not included in our wood density model.

It should be noted that the level of necessary detail in modelled annual mean tree ring density depends on the application. The use in LPJ-GUESS for simulations at the grid cell level does not require a perfect reproduction of the annual tree ring dynamics at site level. It is more important that the wood density model is able to simulate the general trends of increasing and decreasing annual mean wood density as a result of climatic and environmental influences. The wood density model did generally reproduce the density trend across the temperature gradient, however largely overestimated the relative difference between them when phenology was included. An approach to further improve this ability of the model could be to include geography or latitude to also replicate broader geographical effects when the model is applied beyond the scope presented here.

It has been observed that trees in warmer climates produce wood with greater density, and numerous studies conducted in temperate and boreal zones have indicated that wood density increases with temperature. This trend was reproduced by our wood density model. However, this phenomenon does not appear to be consistent. This indicates the phenomenon known as the "Divergence Problem," initially described by D'Arrigo et al. (2008), which describes the observed decline in mean tree ring density since the second half of the 20^{th} century in warming climates (Pretzsch et al., 2018). This effect provides compelling evidence for the integration of a mechanistic model, as a purely empirical model is unable to reproduce such trends. The semi-mechanistic model presented here did not reproduce the reported trend in decreasing mean tree ring density, however such a trend could also not be observed at the validation sites due to limited time periods of the validation data.

LPJ-GUESS-WD demonstrates the significance of incorporating an annually varying wood density in DGVMs. The dynamic wood density influenced tree productivity, carbon distribution across different tree compartments, and overall phenology. Furthermore, the deviation in productivity, age and carbon in leaves and stem were not consistent, with a specific impact resulting from higher or lower wood density compared to the wood density parameter in the standard LPJ-GUESS. The results demonstrated that while mean stem wood density was higher compared to the parameter in the standard version at the two lower elevation sites, productivity and carbon in leaves increased at mid, but decreased at low elevation. These findings support the relevance of wood density in DGVMs, as highlighted by previous research which has

demonstrated its relevance for correctly estimating carbon sequestration and storage in trees and thereby for climate mitigation (Mo et al., 2024, Eitel et al., 2023). Although our results are not directly applicable to carbon storage estimations, our model demonstrates the potential for integrating dynamic wood density into DGVMs. Its relevance is also apparent from the stronger deviations between LPJ-GUESS-WD and the standard LPJ-GUESS from the beginning of the 20^{th} when mean stem wood density started to steeply increase. While the steep increase itself is debatable in the light of the Divergence Problem, the tree growth dynamics show that quick changes in mean stem density trends have a strong impact on productivity and carbon storage. The incorporation of a wood density model thereby can significantly impact carbon storage estimations, which are influenced by the varying residency times of carbon in woody and non-woody biomass. Mean residency time of carbon in trees has been shown to be a key contributor to uncertainties in forest carbon budgets (Friend et al, 2014, Pugh et al., 2020).

The inclusion of dynamic wood density in LPJ-GUESS adds a new capability to the model. Wood density is directly dependent on temperature and growing season, but independent of carbon availability. This integrates partly the temperature sensitivity of stem growth as proposed and previously implemented by Leuzinger et al. (2013). In LPJ-GUESS, growth of stem, roots and leaves is determined by the carbon allocated to them while the allocation is based on the carbon available to the tree's growth. The allocation is focused and solved for the carbon allocated to leaves, resulting in a certain amount of carbon allocated to sapwood. Wood density plays a role in these calculations but has no direct control over the proportion of carbon allocated to the stem. Thereby, the annual stem width gain in diameter is the result of the allocation process and is not directly dependent to environmental factors. Changing the allocation to focus on carbon allocated to the stem, including limiting factors for stem width growth such as temperature and water availability, could further improve carbon storage estimations in trees. Available carbon limiting carbon allocation to the stem is dominant in DGVMs, but some research highlights the benefits of integrated limitations independent of carbon availability (Leuzinger et al., 2013, Franklin et al., 2012, Merganičová et al., 2019).

The integration of the semi-mechanistic dynamic wood density model opens up many opportunities for further research to 1, improve model performance in modelling annual mean wood density and 2, explore its implications in LPJ-GUESS and DGVMs in general. By calibrating the functions to more species, the effects of competition under varying wood density can be investigated. As studies suggest, research on the effect of dynamic wood density on mortality is another field of interest that opens up (Mo et al., 2024, Yang et al., 2024).

Conclusion

This research proposed a temperature-dependent wood density model for the implementation into dynamic global vegetation models. The wood density model did reproduce density trends across elevations but little to no inter-annual mean tree ring density variability. Modelling annual tree ring density could be improved through the implementation of a soil moisture response influencing tree ring phenology. Furthermore, testing of the function across more sites is necessary to identify additional weaknesses. The integration of the wood density model into a dynamic global vegetation model showed the impact of including environmental dependent wood density both for carbon storage estimations and tree traits like height. We suggest that wood density has likely more implications for example for competition and mortality which requires further research. By further developing our wood density model, estimates of carbon storage under the influence of variable wood density can be compared with vegetation model outputs considering a parameterised wood density and observations. Thereby, the contribution of wood density to the reduction of errors in carbon storage estimations can be evaluated.

References

Ackerly, D. (2003). Community assembly, niche conservatism, and adaptive evolution in changing environments. *International Journal of Plant Sciences*, (S3), 165–184. https://doi.org/https://doi.org/10.1086/368401

Beeckman, H. (2016). Wood anatomy and trait-based ecology. *IAWA J.*, *37*, 127–151. https://doi.org/10.1163/22941932-20160127

Begum, S., Kudo, K., Rahman, M., & et al. (2018). Climate change and the regulation of wood formation in trees by temperature. *Trees*, *32*, 3–15. https://doi.org/https://doi.org/10.1007/s00468-017-1587-6

Begum, S., Nakaba, S., Yamagishi, Y., Oribe, Y., & Funada, R. (2013). Regulation of cambial activity in relation to environmental conditions: Understanding the role of temperature in wood formation of trees. *Physiologia plantarum*, *147*(1), 46–54. https://doi.org/https://doi.org/10.1111/j.1399-3054.2012.01663.x

Boakye, E., Mvolo, C., & Stewart, J. (2023). Systematic review: Climate and non-climate factors influencing wood density in the boreal zone. *BioResources*, *18*(4). https://doi.org/10.15376/biores.18.4.Boakye

Buttò, V., Deslauriers, A., & Rossi, S. e. a. (2020). The role of plant hormones in tree-ring formation. *Trees*, *34*, 315–335. https://doi.org/https://doi.org/10.1007/s00468-019-01940-4

Bytebier, J., De Mil, T., Vanhellemont, M., Verheyen, K., Haneca, K., & Van den Bulcke, J. (2022). Linking wood density records of common beech (fagus sylvatica l.) with temperature and precipitation variability from a temperate lowland site. *Dendrochronologia*, *76*. https://doi.org/https://doi.org/10.1016/j.dendro.2022.126018

Camarero, J., Fernández-Pérez, L., Kirdyanov, A., Shestakova, T., Knorre, A., Kukarskih, V., & Voltas, J. (2017). Minimum wood density of conifers portrays changes in early season precipitation at dry and cold eurasian regions. *Trees*, *31*, 1423–1437. https://doi.org/https://doi.org/10.1007/s00468-017-1559-x

Camarero, J., & Hevia, A. (2020). Links between climate, drought and minimum wood density in conifers. *IAWA Journal*, *41*, 1–20. https://doi.org/10.1163/22941932-bja10005

Chave, J., Coomes, D., Jansen, S., Lewis, S., Swenson, N., & Zanne, A. (2009). Towards a worldwide wood economics spectrum. *Ecology Letters*, *12*(4), 351–366. https://doi.org/https://doi.org/10.1111/j.1461-0248.2009.01285.x

Cuny, H., Fonti, P., Rathgeber, C., von Arx, G., Peters, R., & Frank, D. (2019). Couplings in cell differentiation kinetics mitigate air temperature influence on conifer wood anatomy. *Plant, Cell & Environment*, *42*(4), 1222–1232. https://doi.org/https://doi.org/10.1111/pce.13464

Cuny, H., Rathgeber, C., Frank, D., Fonti, P., & Fournier, M. (2014). Kinetics of tracheid development explain conifer tree-ring structure. *New Phytologist*, *203*(4), 1231–1241. https://doi.org/https://doi.org/10.1111/nph.12871

Cuny, H., & Rathgeber, C. (2016). Xylogenesis: Coniferous trees of temperate forests are listening to the climate tale during the growing season but only remember the last words! *Plant physiology*, *171*(1), 306–317. https://doi.org/https://doi.org/10.1104/pp.16.00037

D'Arrigo, R., Wilson, R., Liepert, B., & Cherubini, P. (2008). On the 'divergence problem' in northern forests: A review of the tree-ring evidence and possible causes. *Global and Planetary Change*, *60*(3), 289–305. https://doi.org/https://doi.org/10.1016/j.gloplacha.2007.03.004

Düthorn, E., Schneider, L., Günther, B., Gläser, S., & Esper, J. (2016). Ecological and climatological signals in tree-ring width and density chronologies along a latitudinal boreal transect. *Scandinavian Journal of Forest Research*, *31*(8), 750–757. https://doi.org/10.1080/02827581.2016.1181201

Eckes-Shephard, A. H., Ljungqvist, F. C., Drew, D. M., Rathgeber, C. B. K., & Friend, A. D. (2022). Wood formation modeling - a research review and future perspectives. *Frontiers in plant science*, *13*. https://doi.org/https://doi.org/10.3389/fpls.2022.837648

Eckes-Shephard, A. H., Tiavlovsky, E., Chen, Y., Fonti, P., & Friend, A. D. (2021). Direct response of tree growth to soil water and its implications for terrestrial carbon cycle modelling. *Global Change Biology*, *27*(1), 121–135. https://doi.org/https://doi.org/10.1111/gcb.15397

Eitel, J. U., Basler, D., Braun, S., Buchmann, N., D'Odorico, P., Etzold, S., Gessler, A., Griffin, K. L., Krejza, J., Luo, Y., Maguire, A. J., Rao, M. P., Vitasse, Y., Walthert, L., & Zweifel, R. (2023). Towards monitoring stem growth phenology from space with high resolution satellite data. *Agricultural and Forest Meteorology*, *339*, 109549. https://doi.org/https://doi.org/10.1016/j.agrformet.2023.109549

Franceschini, T., Longuetaud, F., Bontemps, J., Bouriaud, O., Caritey, B., & Leban, J. (2013). Effect of ring width, cambial age, and climatic variables on the within-ring wood density profile of norway spruce picea abies (l.) karst. *Trees*, *27*(4), 913–925. https://doi.org/10.1007/s00468-013-0844-6

Franklin, O., Johansson, J., Dewar, R. C., Dieckmann, U., McMurtrie, R. E., Brännström, A., & Dybzinski, R. (2012). Modeling carbon allocation in trees: A search for principles. *Tree Physiology*, *32*(6), 648–666. https://doi.org/10.1093/treephys/tpr138

Friend, A., Eckes-Shephard, A., & Tupker, Q. (2022). Wood structure explained by complex spatial source-sink interactions. *Nature Communications*, *13*(7824). https://doi.org/https://doi.org/10.1038/s41467-022-35451-7

Friend, A. D., Lucht, W., Rademacher, T. T., Keribin, R., Betts, R., Cadule, P., Ciais, P., Clark, D. B., Dankers, R., Falloon, P. D., Ito, A., Kahana, R., Kleidon, A., Lomas, M. R., Nishina, K., Ostberg, S., Pavlick, R., Peylin, P., Schaphoff, S., … Woodward, F. I. (2014). Carbon residence time dominates uncertainty in terrestrial vegetation responses to future climate and atmospheric co2. *Proceedings of the National Academy of Sciences of the United States of America*, *111*(9), 3280–3285. https://doi.org/10.1073/pnas.1222477110

Fritts, H. (1976). Chapter 1 - dendrochronology and dendroclimatology. In H. Fritts (Ed.), *Tree rings and climate* (pp. 1–54). Academic Press. https://doi.org/https://doi.org/10.1016/B978-0-12-268450-0.50006-9

Gričar, J., Čufar, K., Eler, K., Gryc, V., Vavrčík, H., de Luis, M., & Prislan, P. (2021). Transition dates from earlywood to latewood and early phloem to late phloem in norway spruce. *Forests*, *12*(3). https://doi.org/10.3390/f12030331

Gričar, J., Zupančič, M., Čufar, K., Koch, G., Schmitt, U., & Oven, P. (2006). Effect of local heating and cooling on cambial activity and cell differentiation in the stem of norway spruce (picea abies). *Annals of botany*, *97*(6), 943–951. https://doi.org/https://doi.org/10.1093/aob/mcl050

He, M., Yang, B., Shishov, V., Rossi, S., Bräuning, A., Ljungqvist, F. C., & Grießinger, J. (2018). Relationships between wood formation and cambium phenology on the tibetan plateau during 1960–2014. *Forests*, *9*(2). https://doi.org/10.3390/f9020086

Leuzinger, S., Manusch, C., Bugmann, H., & Wolf, A. (2013). A sink-limited growth model improves biomass estimation along boreal and alpine tree lines. *Global Ecology and Biogeography*, *22*. https://doi.org/10.1111/geb.12047

Levanič, T., Gričar, J., Gagen, M., Jalkanen, R., Loader, N. J., McCarroll, D., Oven, P., & Robertson, I. (2009). The climate sensitivity of norway spruce [picea abies (l.) karst.] in the southeastern european alps. *Trees*, *23*, 169–180. https://doi.org/https://doi.org/10.1007/s00468-008-0265-0

Lupi, C., Morin, H., Deslauriers, A., & Rossi, S. (2010). Xylem phenology and wood production: Resolving the chicken-or-egg dilemma. *Plant, cell and environment*, *33*(10), 1721–1730. https://doi.org/https://doi.org/10.1111/j.1365-3040.2010.02176.x

Matras, J., & Pâques, L. (2003). Euforgen technical guidelines for genetic conservation and use for european larch ((larix decidua)). Retrieved April 29, 2024, from https://www.euforgen.org/species/larix-decidua/

Mencuccini, M., Rosas, T., Rowland, L., Choat, B., Cornelissen, H., Jansen, S., Kramer, K., Lapenis, A., Manzoni, S., Niinemets, Ü., Reich, P. B., Schrodt, F., Soudzilovskaia, N., Wright, I. J., & Martínez-Vilalta, J. (2019). Leaf economics and plant hydraulics drive leaf : Wood area ratios. *New Phytologist*, *224*(4), 1544–1556. https://doi.org/https://doi.org/10.1111/nph.15998

Merganičová, K., Merganič, J., Lehtonen, A., Vacchiano, G., Sever, M. Z. O., Augustynczik, A. L., Grote, R., Kyselová, I., Mäkelä, A., Yousefpour, R., Krejza, J., Collalti, A., & Reyer, C. P. (2019). Forest carbon allocation modelling under climate change. *Tree Physiology*, *39*(12), 1937–1960. https://doi.org/10.1093/treephys/tpz105

Micco, V. D., Carrer, M., Rathgeber, C. B., Camarero, J. J., Voltas, J., Cherubini, P., & Battipaglia, G. (2019). From xylogenesis to tree rings: Wood traits to investigate tree response to environmental changes. *IAWA Journal*, *40*(2), 155–182. https://doi.org/10.1163/22941932-40190246

Mo, L., Crowther, T., & et al., D. M. (2024). Consistent climatic controls of global wood density among angiosperms and gymnosperms. *PREPRINT (Version 1)*. https://doi.org/https://doi.org/10.21203/rs.3.rs-3934396/v1

National Oceanic and Atmospheric Administration (NOAA). (2022). *International tree-ring data bank (itrdb), version 8.0*. Retrieved February 2, 2024, from https://www.ncei.noaa.gov/products/paleoclimatology/tree-ring

Ogle, K., Pathikonda, S., Sartor, K., Lichstein, J., Osnas, J., & Pacala, S. (2014). A model-based meta-analysis for estimating species-specific wood density and identifying potential sources of variation. *Journal of Ecology*, *102*(1), 194–208. https://doi.org/https://doi.org/10.1111/1365-2745.12178

Oribe, Y., & Kubo, T. (1997). Effect of heat on cambial reactivation during winter dormancy in evergreen and deciduous conifers. *Tree physiology*, *17*(2), 81–87. https://doi.org/https://doi.org/10.1093/treephys/17.2.81

Oribe, Y., Funada, R., Shibagaki, M., & Kubo, T. (2001). Cambial reactivation in locally heated stems of the evergreen conifer abies sachalinensis (schmidt) masters. *Planta*, *212*(5/6), 684–691. Retrieved May 1, 2024, from http://www.jstor.org/stable/23386161

Pan, Y., Birdsey, R. A., Fang, J., Houghton, R., Kauppi, P. E., Kurz, W. A., Phillips, O. L., Shvidenko, A., Lewis, S. L., Canadell, J. G., Ciais, P., Jackson, R. B., Pacala, S. W., McGuire, A. D., Piao, S., Rautiainen, A., Sitch, S., & Hayes, D. (2011). A large and persistent carbon sink in the world's forests. *Science*, *333*(6045), 988–993. https://doi.org/10.1126/science.1201609

Parton, W. J. (1996). The century model. In D. S. Powlson, P. Smith, & J. U. Smith (Eds.), *Evaluation of soil organic matter models* (pp. 283–291). Springer Berlin Heidelberg.

Pretzsch, H., Biber, P., Schütze, G., Kemmerer, J., & Uhl, E. (2018). Wood density reduced while wood volume growth accelerated in central european forests since 1870. *Forest Ecology and Management*, *429*, 589–616. https://doi.org/https://doi.org/10.1016/j.foreco.2018.07.045

Pritzkow, C., Heinrich, I., Grudd, H., & Helle, G. (2014). Relationship between wood anatomy, tree-ring widths and wood density of pinus sylvestris l. and climate at high latitudes in

northern sweden. *Dendrochronologia*, *32*(4), 295–302. https://doi.org/https://doi.org/10.1016/j.dendro.2014.07.003

Pugh, T. A. M., Rademacher, T., Shafer, S. L., Steinkamp, J., Barichivich, J., Beckage, B., Haverd, V., Harper, A., Heinke, J., Nishina, K., Rammig, A., Sato, H., Arneth, A., Hantson, S., Hickler, T., Kautz, M., Quesada, B., Smith, B., & Thonicke, K. (2020). Understanding the uncertainty in global forest carbon turnover. *Biogeosciences*, *17*(15), 3961–3989. https://doi.org/10.5194/bg-17-3961-2020

Rathgeber, C. (2017). Conifer tree-ring density inter-annual variability – anatomical, physiological and environmental determinants. *New Phytologist*, *216*(3), 621–625. https://doi.org/10.1111/nph.14763

Rosell, J., Olson, M., & Anfodillo, T. (2017). Scaling of xylem vessel diameter with plant size: Causes, predictions, and outstanding questions. *Currrent Forestry Reports*, *3*, 46–59. https://doi.org/https://doi.org/10.1007/s40725-017-0049-0

Rossi, S., Girard, M.-J., & Morin, H. (2014). Lengthening of the duration of xylogenesis engenders disproportionate increases in xylem production. *Global Change Biology*, *20*(7), 2261–2271. https://doi.org/10.1111/gcb.12470

Smith, B., Prentice, C., & Skyes, M. T. (2001). Represntation of vegetation dynamics in the modelling of terrestrial ecosystems: Comparing two contrasting approaches within european climate space. *Global Ecology and Biogeography*, *10*(6), 621–637. https://doi.org/10.1046/j.1466-822X.2001.t01-1-00256.x

Smith, B., Wårlind, D., Arneth, A., Hickler, T., Leadley, P., Siltberg, J., & Zaehle, S. (2014). Implications of incorporating n cycling and n limitations on primary production in an individual-based dynamic vegetation model. *Biogeosciences*, *11*(7), 2027–2054. https://doi.org/10.5194/bg-11-2027-2014

University of East Anglia Climatic Research Unit, I., Harris. (2020). *Cru jra v2.1: A forcings dataset of gridded land surface blend of climatic research unit (cru) and japanese reanalysis (jra) data and jan. 1901 - dec. 2019*. Centre for Environmental Data Analysis. Retrieved January 25, 2024, from https://catalogue.ceda.ac.uk/uuid/10d2c73e5a7d46f4ada08b0a26302ef7

van der Maaten, E., van der Maaten-Theunissen, M., & Spiecker, H. (2012). Temporally resolved intra-annual wood density variations in european beech (fagus sylvatica l.) as affected by climate and aspect. *Annaly of forest research*, *55*(1). https://doi.org/https://doi.org/10.15287/afr.2012.83

Wang, W., Zhu, M., Lin, L., Yang, Z., & Yao, F. (2023). The early- to latewood transition phenology is asynchronous between the different parts of abies forrestii var. smithii in jiaozi mountain, yunnan, china. *Forests*, *14*(7). https://doi.org/10.3390/f14071456

Yang, H., Wang, S., Son, R., Lee, H., Benson, V., Zhang, W., Zhang, Y., Zhang, Y., Kattge, J., Boenisch, G., Schepaschenko, D., Karaszewski, Z., Stereńczak, K., Moreno-Martínez, Á.,

Nabais, C., Birnbaum, P., Vieilledent, G., Weber, U., & Carvalhais, N. (2024). Global patterns of tree wood density. *Global Change Biology*, *30*(3), e17224. https://doi.org/https://doi.org/10.1111/gcb.17224

Appendix B: Supplementary Material

B1 Supplementary Material to Methods and Data

B1.1 | ITRDB data

All data for the function building was retrieved from the International Tree Ring Data Base (ITRDB) (National Oceanic and Atmospheric Administration (NOAA), 2022). Only sites for which earlywood width and density and latewood width and density were available were considered. The data stemmed from a total of 84 sites primarily in Russia with one in Switzerland (detailed list of all sites and data origin in Tab. B1). The data includes three larch species, European larch (*Larix decidua*), Dahurian larch (*Larix gmelinii*) and Siberian larch (*Larix sibirica*). The sites' location spanned from 46°N to 73°N and from 3.5°W to 169°E (Fig. B1). Elevations varied from 0 to 2150 m above sea level. Information and references to all data sets are shown in Tab. B1.

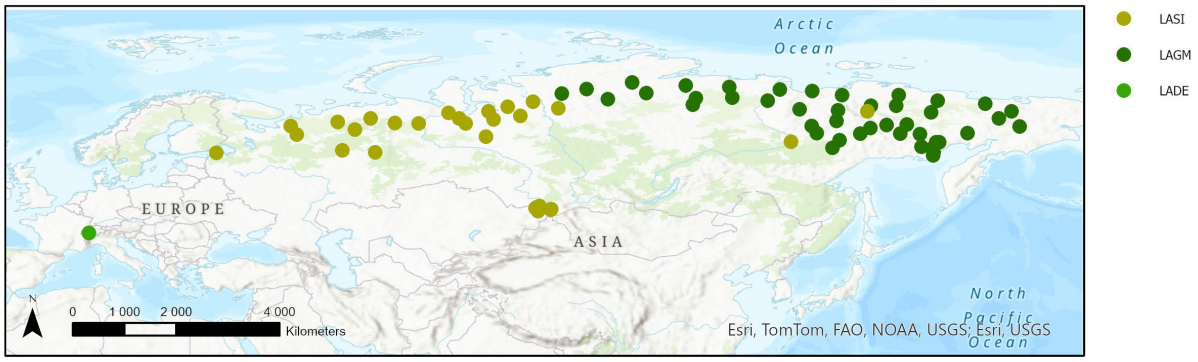

Figure B1: Map of all sites from which observations contributed to the function building for the dynamic wood density model. The species included are European Larch (*Larix decidua*, LADE), Dahurian larch (*Larix gmelinii*, LAGM) and Siberian larch (*Larix sibirica*, LASI).

The data was first averaged per site and year for each of the variables and filtered to include only years within 1901-1999 resulting in overall 7334 data-points representing site-year pairings. All site-year pairings were removed where at least one variable had a z-score greater than three. Z-scores were calculated as:

$$z = \frac{v_{s,y} - \overline{v}}{\sigma_V} \tag{B1}$$

where $v_{s,y}$ is the value of a specific site and year to be z-scored, $\overline{v}$ is the mean and σ_V is the

standard deviation of that variable across all sites and years. Overall, 510 values were removed due to z-scoring leaving 6824 site-year pairings used for function building.

Table B1: Sites used for the function building retrieved from the ITRDB (National Oceanic and Atmospheric Administration (NOAA), 2022). LAGM = Dahurian Larch (*Larix gmelinii*), LASI = Sibirian Larch (*Larix sibirica*), European Larch (*Larix decidua*). EWW = earlywood width, EWD = earlywood density, LWW = latewood width, LWD = latewood density.

Site	Coordinates	Elevation	Species	Variables	Reference
RUSS023	66.67 N, 82.33 E	15 m	LASI	EWW, EWD, LWW, LWD	Schweingruber, F.H. (2002-05-29): NOAA/WDS Paleoclimatology - Schweingruber - Sidorovsk - LASI - ITRDB RUSS023. NOAA National Centers for Environmental Information. https://doi.org/10.25921/d3pg-ge50. Accessed 2024-05-04.
RUSS024	70.6 N, 104.25 E	130 m	LAGM	EWW, EWD, LWW, LWD	Schweingruber, F.H. (2002-05-29): NOAA/WDS Paleoclimatology - Schweingruber - Kotuykan River B - LAGM - ITRDB RUSS024. NOAA National Centers for Environmental Information. https://doi.org/10.25921/xdbx-s906. Accessed 2024-05-04.
RUSS025	69.78 N, 119.12 E	130 m	LAGM	EWW, EWD, LWW, LWD	Schweingruber, F.H. (2002-05-28): NOAA/WDS Paleoclimatology - Schweingruber - Olenok River - LAGM - ITRDB RUSS025. NOAA National Centers for Environmental Information. https://doi.org/10.25921/q2sz-y826. Accessed 2024-05-04.
RUSS027	68.25 N, 80.18 E	60 m	LASI	EWW, EWD, LWW, LWD	Schweingruber, F.H. (2002-05-29): NOAA/WDS Paleoclimatology - Schweingruber - Indikyakha-River - LASI - ITRDB RUSS027. NOAA National Centers for Environmental Information. https://doi.org/10.25921/r57g-rg48. Accessed 2024-05-04.
RUSS028	67.97 N, 88.92 W	160 m	LASI	LWW, LWD, EWW, EWD	Schweingruber, F.H. (2002-05-29): NOAA/WDS Paleoclimatology - Schweingruber - Kulyumbe River - LASI - ITRDB RUSS028. NOAA National Centers for Environmental Information. https://doi.org/10.25921/e3qp-7529. Accessed 2024-05-04.

RUSS029	70.52 N, 89.5 E	50 m	LAGM	EWW, EWD, LWW, LWD	Schweingruber, F.H. (2002-05-29): NOAA/WDS Paleoclimatology - Schweingruber - Ikon River - LAGM - ITRDB RUSS029. NOAA National Centers for Environmental Information. https://doi.org/10.25921/f87r-2n62. Accessed 2024-05-04.
RUSS035	67.2 N, 69.83 E	90 m	LASI	EWW, EWD, LWW, LWD	Schweingruber, F.H. (2005-04-12): NOAA/WDS Paleoclimatology - Schweingruber - Khadyta River - LASI - ITRDB RUSS035. NOAA National Centers for Environmental Information. https://doi.org/10.25921/by0d-gh05. Accessed 2024-05-04.
RUSS044	63.43 N, 43.55 E	120 m	LASI	EWW, EWD, LWW, LWD	Schweingruber, F.H. (2002-05-28): NOAA/WDS Paleoclimatology - Schweingruber - Voroney - LASI - ITRDB RUSS044. NOAA National Centers for Environmental Information. https://doi.org/10.25921/40cn-6a60. Accessed 2024-05-04.
RUSS048	68.6 N, 112.25 E	300 m	LAGM	EWW, EWD, LWW, LWD	Schweingruber, F.H. (2005-08-25): NOAA/WDS Paleoclimatology - Schweingruber - Olenjok - LAGM - ITRDB RUSS048. NOAA National Centers for Environmental Information. https://doi.org/10.25921/0hbs-6125. Accessed 2024-05-04.
RUSS053	67.45 N, 142.62 E	100 m	LASI	EWW, EWD, LWW, LWD	Schweingruber, F.H. (2005-04-13): NOAA/WDS Paleoclimatology - Schweingruber - Zhaschiviersk - LASI - ITRDB RUSS053. NOAA National Centers for Environmental Information. https://doi.org/10.25921/fkbj-p165. Accessed 2024-05-04.
RUSS059	69.28 N, 125.33 E	130 m	LAGM	EWW, EWD, LWW, LWD	Schweingruber, F.H. (2005-04-13): NOAA/WDS Paleoclimatology - Schweingruber - Uel-Siktjach river - LAGM - ITRDB RUSS059. NOAA National Centers for Environmental Information. https://doi.org/10.25921/kby3-1955. Accessed 2024-05-04.
RUSS061	64.25 N, 53.57 E	70 m	LASI	EWW, EWD, LWW, LWD	Schweingruber, F.H. (2002-05-28): NOAA/WDS Paleoclimatology - Schweingruber - Kedvaran - LASI - ITRDB RUSS061. NOAA National Centers for Environmental Information. https://doi.org/10.25921/6h4n-b824. Accessed 2024-05-04.

RUSS063	68.42 N, 143.17 E	45 m	LAGM	EWW, EWD, LWW, LWD	Schweingruber, F.H. (2002-05-28): NOAA/WDS Paleoclimatology - Schweingruber - Ayandina River - LAGM - ITRDB RUSS063. NOAA National Centers for Environmental Information. https://doi.org/10.25921/evmt-ps03. Accessed 2024-05-04.
RUSS064	66.22 N, 56.33 E	65 m	LASI	EWW, EWD, LWW, LWD	Schweingruber, F.H. (2005-04-13): NOAA/WDS Paleoclimatology - Schweingruber - Shchely Bozh - LASI - ITRDB RUSS064. NOAA National Centers for Environmental Information. https://doi.org/10.25921/0e3r-6m43. Accessed 2024-05-04.
RUSS066	64.47 N, 137.75 E	400 m	LAGM	EWW, EWD, LWW, LWD	Schweingruber, F.H. (2005-04-13): NOAA/WDS Paleoclimatology - Schweingruber - Khandiga River - LAGM - ITRDB RUSS066. NOAA National Centers for Environmental Information. https://doi.org/10.25921/t53b-1s22. Accessed 2024-05-04.
RUSS069	69.77 N, 112.82 E	150 m	LAGM	EWW, EWD, LWW, LWD	Schweingruber, F.H. (2002-05-28): NOAA/WDS Paleoclimatology - Schweingruber - Kuonamka River (feucht) - LAGM - ITRDB RUSS069. NOAA National Centers for Environmental Information. https://doi.org/10.25921/yz3e-6z49. Accessed 2024-05-04.
RUSS070	63.52 N, 151.72 E	450 m	LAGM	EWW, EWD, LWW, LWD	Schweingruber, F.H. (2002-05-28): NOAA/WDS Paleoclimatology - Schweingruber - Seimchan-river - LAGM - ITRDB RUSS070. NOAA National Centers for Environmental Information. https://doi.org/10.25921/jv36-y686. Accessed 2024-05-04.
RUSS075	60.7 N, 51.38 E	160 m	LASI	EWW, EWD, LWW, LWD	Schweingruber, F.H. (2002-05-28): NOAA/WDS Paleoclimatology - Schweingruber - Nyuchpas - LASI - ITRDB RUSS075. NOAA National Centers for Environmental Information. https://doi.org/10.25921/q420-nm39. Accessed 2024-05-04.
RUSS076	71.9 N, 111.03 E	150 m	LAGM	EWW, EWD, LWW, LWD	Schweingruber, F.H. (2002-05-28): NOAA/WDS Paleoclimatology - Schweingruber - Popigay - LAGM - ITRDB RUSS076. NOAA National Centers for Environmental Information. https://doi.org/10.25921/1k51-b754. Accessed 2024-05-04.

RUSS077	71.7 N, 118.58 E	140 m	LAGM	EWW, EWD, LWW, LWD	Schweingruber, F.H. (2002-05-28): NOAA/WDS Paleoclimatology - Schweingruber - Ary-Ongorbynf-River A - LAGM - ITRDB RUSS077. NOAA National Centers for Environmental Information. https://doi.org/10.25921/xg1r-vh06. Accessed 2024-05-04.
RUSS078	69.12 N, 84.5 E	80 m	LASI	EWW, EWD, LWW, LWD	Schweingruber, F.H. (2002-05-28): NOAA/WDS Paleoclimatology - Schweingruber - Kheta River - LASI - ITRDB RUSS078. NOAA National Centers for Environmental Information. https://doi.org/10.25921/rsyb-gq62. Accessed 2024-05-04.
RUSS079	69.12 N, 84.5 W	80 m	LASI	EWW, EWD, LWW, LWD	Schweingruber, F.H. (2002-05-28): NOAA/WDS Paleoclimatology - Schweingruber - Kheta River junge Bäume - LASI - ITRDB RUSS079. NOAA National Centers for Environmental Information. https://doi.org/10.25921/7xhb-6w34. Accessed 2024-05-04.
RUSS080	72.45 N, 101.75 E	70 m	LAGM	EWW, EWD, LWW, LWD	Schweingruber, F.H. (2002-05-29): NOAA/WDS Paleoclimatology - Schweingruber - Novoja Rieka - LAGM - ITRDB RUSS080. NOAA National Centers for Environmental Information. https://doi.org/10.25921/e9gt-w192. Accessed 2024-05-04.
RUSS082	66.08 N, 77.68 E	30 m	LASI	EWW, EWD, LWW, LWD	Schweingruber, F.H. (2002-05-28): NOAA/WDS Paleoclimatology - Schweingruber - Yevoyakha River - LASI - ITRDB RUSS082. NOAA National Centers for Environmental Information. https://doi.org/10.25921/qwwd-2e68. Accessed 2024-05-04.
RUSS084	65.38 N, 72.87 E	100 m	LASI	EWW, EWD, LWW, LWD	Schweingruber, F.H. (2005-04-13): NOAA/WDS Paleoclimatology - Schweingruber - Kheygiyakha River B - LASI - ITRDB RUSS084. NOAA National Centers for Environmental Information. https://doi.org/10.25921/g09e-z189. Accessed 2024-05-04.
RUSS086	61.15 N, 136.57 E	600 m	LAGM	EWW, EWD, LWW, LWD	Schweingruber, F.H. (2002-05-29): NOAA/WDS Paleoclimatology - Schweingruber - Tschuchonoi River - LAGM - ITRDB RUSS086. NOAA National Centers for Environmental Information. https://doi.org/10.25921/vwjb-6019. Accessed 2024-05-04.

RUSS087	68.45 N, 147.58 E	140 m	LAGM	EWW, EWD, LWW, LWD	Schweingruber, F.H. (2005-04-13): NOAA/WDS Paleoclimatology - Schweingruber - Alagea River - LAGM - ITRDB RUSS087. NOAA National Centers for Environmental Information. https://doi.org/10.25921/h033-xq30. Accessed 2024-05-04.
RUSS088	66.22 N, 165.42 E	500 m	LAGM	EWW, EWD, LWW, LWD	Schweingruber, F.H. (2002-05-28): NOAA/WDS Paleoclimatology - Schweingruber - Balshoia Anui - LAGM - ITRDB RUSS088. NOAA National Centers for Environmental Information. https://doi.org/10.25921/bxh9-ft09. Accessed 2024-05-04.
RUSS089	65.1 N, 154.93 E	150 m	LAGM	EWW, EWD, LWW, LWD	Schweingruber, F.H. (2005-08-25): NOAA/WDS Paleoclimatology - Schweingruber - Bulun river - LAGM - ITRDB RUSS089. NOAA National Centers for Environmental Information. https://doi.org/10.25921/119a-j328. Accessed 2024-05-04.
RUSS090	64.53 N, 143.12 E	600 m	LAGM	EWW, EWD, LWW, LWD	Schweingruber, F.H. (2002-05-29): NOAA/WDS Paleoclimatology - Schweingruber - Ust Nera - LAGM - ITRDB RUSS090. NOAA National Centers for Environmental Information. https://doi.org/10.25921/7pd1-a294. Accessed 2024-05-04.
RUSS091	65.15 N, 149.43 E	300 m	LAGM	EWW, EWD, LWW, LWD	Schweingruber, F.H. (2002-05-28): NOAA/WDS Paleoclimatology - Schweingruber - Rossocha River - LAGM - ITRDB RUSS091. NOAA National Centers for Environmental Information. https://doi.org/10.25921/bdmb-hd79. Accessed 2024-05-04.
RUSS092	67.47 N, 76.77 E	20 m	LASI	EWW, EWD, LWW, LWD	Schweingruber, F.H. (2002-05-29): NOAA/WDS Paleoclimatology - Schweingruber - Khadutte River - LASI - ITRDB RUSS092. NOAA National Centers for Environmental Information. https://doi.org/10.25921/zzsv-f694. Accessed 2024-05-04.
RUSS094	69.53 N, 97.53 E	550 m	LAGM	EWW, EWD, LWW, LWD	Schweingruber, F.H. (2002-05-29): NOAA/WDS Paleoclimatology - Schweingruber - Ayakli River A - LAGM - ITRDB RUSS094. NOAA National Centers for Environmental Information. https://doi.org/10.25921/dhtr-qn62. Accessed 2024-05-04.

RUSS098	64.92 N, 42.5 E	230 m	LASI	EWW, EWD, LWW, LWD	Schweingruber, F.H. (2002-05-29): NOAA/WDS Paleoclimatology - Schweingruber - Pinega, Belomop-kuloi pla - LASI - ITRDB RUSS098. NOAA National Centers for Environmental Information. https://doi.org/10.25921/sq7y-n611. Accessed 2024-05-04.
RUSS101	66.22 N, 71.67 E	80 m	LASI	EWW, EWD, LWW, LWD	Schweingruber, F.H. (2002-05-29): NOAA/WDS Paleoclimatology - Schweingruber - Nadim River - LASI - ITRDB RUSS101. NOAA National Centers for Environmental Information. https://doi.org/10.25921/p80g-a511. Accessed 2024-05-04.
RUSS102	67.25 N, 153.7 E	50 m	LAGM	EWW, EWD, LWW, LWD	Schweingruber, F.H. (2002-05-28): NOAA/WDS Paleoclimatology - Schweingruber - Srednie-Kolymsk - LAGM - ITRDB RUSS102. NOAA National Centers for Environmental Information. https://doi.org/10.25921/k5re-nk84. Accessed 2024-05-04.
RUSS103	64.93 N, 132.93 E	750 m	LAGM	EWW, EWD, LWW, LWD	Schweingruber, F.H. (2002-05-29): NOAA/WDS Paleoclimatology - Schweingruber - Sartan river - LAGM - ITRDB RUSS103. NOAA National Centers for Environmental Information. https://doi.org/10.25921/wzxe-ah32. Accessed 2024-05-04.
RUSS105	63.62 N, 141.35 E	750 m	LAGM	EWW, EWD, LWW, LWD	Schweingruber, F.H. (2002-05-29): NOAA/WDS Paleoclimatology - Schweingruber - Bryungjade river - LAGM - ITRDB RUSS105. NOAA National Centers for Environmental Information. https://doi.org/10.25921/faax-wc13. Accessed 2024-05-04.
RUSS106	70.25 N, 138.17 E	80 m	LAGM	EWW, EWD, LWW, LWD	Schweingruber, F.H. (2002-05-29): NOAA/WDS Paleoclimatology - Schweingruber - Batagay,Chandon-river - LAGM - ITRDB RUSS106. NOAA National Centers for Environmental Information. https://doi.org/10.25921/bcph-9816. Accessed 2024-05-04.
RUSS107	68.8 N, 163.05 E	300 m	LAGM	EWW, EWD, LWW, LWD	Schweingruber, F.H. (2002-05-28): NOAA/WDS Paleoclimatology - Schweingruber - Cherskij - LAGM - ITRDB RUSS107. NOAA National Centers for Environmental Information. https://doi.org/10.25921/5b1h-h642. Accessed 2024-05-04.

RUSS108	63.65 N, 133.78 E	200 m	LAGM	EWW, EWD, LWW, LWD	Schweingruber, F.H. (2002-05-29): NOAA/WDS Paleoclimatology - Schweingruber - Baraii River - LAGM - ITRDB RUSS108. NOAA National Centers for Environmental Information. https://doi.org/10.25921/s4nj-vx80. Accessed 2024-05-04.
RUSS110	67.83 N, 130.83 E	750 m	LAGM	EWW, EWD, LWW, LWD	Schweingruber, F.H. (2002-05-28): NOAA/WDS Paleoclimatology - Schweingruber - Verchoyansk,Cakker river - LAGM - ITRDB RUSS110. NOAA National Centers for Environmental Information. https://doi.org/10.25921/e7km-5w91. Accessed 2024-05-04.
RUSS111	63.58 N, 148.28 E	1000 m	LAGM	EWW, EWD, LWW, LWD	Schweingruber, F.H. (2002-05-29): NOAA/WDS Paleoclimatology - Schweingruber - Shaguchan river - LAGM - ITRDB RUSS111. NOAA National Centers for Environmental Information. https://doi.org/10.25921/097c-1r45. Accessed 2024-05-04.
RUSS112	62.22 N, 129.35 E	270 m	LASI	EWW, EWD, LWW, LWD	Schweingruber, F.H. (2002-05-28): NOAA/WDS Paleoclimatology - Schweingruber - Yakutsk Biol.Station - LASI - ITRDB RUSS112. NOAA National Centers for Environmental Information. https://doi.org/10.25921/6a5j-4c89. Accessed 2024-05-04.
RUSS113	67.62 N, 137.47 E	350 m	LAGM	EWW, EWD, LWW, LWD	Schweingruber, F.H. (2002-05-29): NOAA/WDS Paleoclimatology - Schweingruber - Tirekhtjakh river - LAGM - ITRDB RUSS113. NOAA National Centers for Environmental Information. https://doi.org/10.25921/vch4-0r48. Accessed 2024-05-04.
RUSS114	70.95 N, 132.98 E	20 m	LAGM	EWW, EWD, LWW, LWD	Schweingruber, F.H. (2002-05-29): NOAA/WDS Paleoclimatology - Schweingruber - Omoloya River - LAGM - ITRDB RUSS114. NOAA National Centers for Environmental Information. https://doi.org/10.25921/6fhc-da82. Accessed 2024-05-04.
RUSS115	60.27 N, 29.58 E	20 m	LASI	EWW, EWD, LWW, LWD	Schweingruber, F.H. (2002-05-29): NOAA/WDS Paleoclimatology - Schweingruber - Lindulowo - LASI - ITRDB RUSS115. NOAA National Centers for Environmental Information. https://doi.org/10.25921/d6n6-xs87. Accessed 2024-05-04.

RUSS117	60.38 N, 57.12 E	140 m	LASI	EWW, EWD, LWW, LWD	Schweingruber, F.H. (2002-05-29): NOAA/WDS Paleoclimatology - Schweingruber - Krasnovishersk - LASI - ITRDB RUSS117. NOAA National Centers for Environmental Information. https://doi.org/10.25921/8fxj-tz11. Accessed 2024-05-04.
RUSS119	65.6 N, 50.63 E	70 m	LASI	EWW, EWD, LWW, LWD	Schweingruber, F.H. (2002-05-28): NOAA/WDS Paleoclimatology - Schweingruber - Nonburg - LASI - ITRDB RUSS119. NOAA National Centers for Environmental Information. https://doi.org/10.25921/ft3y-e177. Accessed 2024-05-04.
RUSS122	66.08 N, 77.68 E	50 m	LASI	EWW, EWD, LWW, LWD	Schweingruber, F.H. (2002-05-28): NOAA/WDS Paleoclimatology - Schweingruber - Malchoyakha River - LASI - ITRDB RUSS122. NOAA National Centers for Environmental Information. https://doi.org/10.25921/dsmx-8f48. Accessed 2024-05-04.
RUSS123	65.45 N, 60.58 E	400 m	LASI	EWW, EWD, LWW, LWD	Schweingruber, F.H. (2002-05-28): NOAA/WDS Paleoclimatology - Schweingruber - Kozhim - LASI - ITRDB RUSS123. NOAA National Centers for Environmental Information. https://doi.org/10.25921/axh5-y162. Accessed 2024-05-04.
RUSS124	71.33 N, 93.83 E	60 m	LAGM	EWW, EWD, LWW, LWD	Schweingruber, F.H. (2002-05-29): NOAA/WDS Paleoclimatology - Schweingruber - Balschaya Kamenka River - LAGM - ITRDB RUSS124. NOAA National Centers for Environmental Information. https://doi.org/10.25921/b7pf-dm10. Accessed 2024-05-04.
RUSS126	67.47 N, 167.67 E	450 m	LAGM	EWW, EWD, LWW, LWD	Schweingruber, F.H. (2002-05-28): NOAA/WDS Paleoclimatology - Schweingruber - Bilibina, Mali Anuj River - LAGM - ITRDB RUSS126. NOAA National Centers for Environmental Information. https://doi.org/10.25921/n4yg-n171. Accessed 2024-05-04.
RUSS127	50.15 N, 85.37 E	1750 m	LASI	EWW, EWD, LWW, LWD	Schweingruber, F.H. (2002-05-28): NOAA/WDS Paleoclimatology - Schweingruber - Ust Koksa Hill (Altai) - LASI - ITRDB RUSS127. NOAA National Centers for Environmental Information. https://doi.org/10.25921/9m4w-bw55. Accessed 2024-05-04.

RUSS129	51 N, 85.63 E	1450 m	LASI	EWW, EWD, LWW, LWD	Schweingruber, F.H. (2002-05-29): NOAA/WDS Paleoclimatology - Schweingruber - Ceminsky pass (Altai) - LASI - ITRDB RUSS129. NOAA National Centers for Environmental Information. https://doi.org/10.25921/7ypj-4y17. Accessed 2024-05-04.
RUSS130	50.87 N, 85.23 E	1450 m	LASI	EWW, EWD, LWW, LWD	Schweingruber, F.H. (2002-05-28): NOAA/WDS Paleoclimatology - Schweingruber - Jablonsky P. east Altai - LASI - ITRDB RUSS130. NOAA National Centers for Environmental Information. https://doi.org/10.25921/491z-ww77. Accessed 2024-05-04.
RUSS132	6928 N, 154.77 E	50 m	LAGM	EWW, EWD, LWW, LWD	Schweingruber, F.H. (2002-05-28): NOAA/WDS Paleoclimatology - Schweingruber - Andryuschkine - LAGM - ITRDB RUSS132. NOAA National Centers for Environmental Information. https://doi.org/10.25921/56ej-2w09. Accessed 2024-05-04.
RUSS133	50.5 N, 87.68 E	1950 m	LASI	EWW, EWD, LWW, LWD	Schweingruber, F.H. (2002-05-28): NOAA/WDS Paleoclimatology - Schweingruber - Ust Ulagan Bog (Altai) - LASI - ITRDB RUSS133. NOAA National Centers for Environmental Information. https://doi.org/10.25921/r4a0-4z39. Accessed 2024-05-04.
RUSS134	61.28 N, 151.95 E	900 m	LAGM	EWW, EWD, LWW, LWD	Schweingruber, F.H. (2002-05-29): NOAA/WDS Paleoclimatology - Schweingruber - Majakit River/village - LAGM - ITRDB RUSS134. NOAA National Centers for Environmental Information. https://doi.org/10.25921/c7y3-sv55. Accessed 2024-05-04.
RUSS135	50.42 N, 87.58 E	2000 m	LASI	EWW, EWD, LWW, LWD	Schweingruber, F.H. (2002-05-28): NOAA/WDS Paleoclimatology - Schweingruber - Aktasch Valley (Altai) - LASI - ITRDB RUSS135. NOAA National Centers for Environmental Information. https://doi.org/10.25921/dpsm-mm81. Accessed 2024-05-04.

RUSS136	50.87 N, 85.23 E	1400 m	LASI	EWW, EWD, LWW, LWD	Schweingruber, F.H. (2002-05-28): NOAA/WDS Paleoclimatology - Schweingruber - Jablonsky P. west Altai - LASI - ITRDB RUSS136. NOAA National Centers for Environmental Information. https://doi.org/10.25921/b4zg-yp11. Accessed 2024-05-04.
RUSS137	50.48 N, 87.65 E	2150 m	LASI	EWW, EWD, LWW, LWD	Schweingruber, F.H. (2002-05-29): NOAA/WDS Paleoclimatology - Schweingruber - Ust Ulagan Lake (Altai) - LASI - ITRDB RUSS137. NOAA National Centers for Environmental Information. https://doi.org/10.25921/vy4d-8b36. Accessed 2024-05-04.
RUSS138	61.17 N, 153.97 E	-	LAGM	EWW, EWD, LWW, LWD	Schweingruber, F.H. (2002-05-28): NOAA/WDS Paleoclimatology - Schweingruber - Julietta north - LAGM - ITRDB RUSS138. NOAA National Centers for Environmental Information. https://doi.org/10.25921/yedy-kc22. Accessed 2024-05-04.
RUSS140	50.65 N, 84.98 E	1500 m	LASI	EWW, EWD, LWW, LWD	Schweingruber, F.H. (2002-05-29): NOAA/WDS Paleoclimatology - Schweingruber - Kirisky Pass (Altai) - LASI - ITRDB RUSS140. NOAA National Centers for Environmental Information. https://doi.org/10.25921/786q-r692. Accessed 2024-05-04.
RUSS141	63.67 N, 159.95 E	800 m	LAGM	EWW, EWD, LWW, LWD	Schweingruber, F.H. (2002-05-29): NOAA/WDS Paleoclimatology - Schweingruber - Kubaka upper near timber - LAGM - ITRDB RUSS141. NOAA National Centers for Environmental Information. https://doi.org/10.25921/f72a-0b69. Accessed 2024-05-04.
RUSS142	70.28 N, 148.05 E	50 m	LAGM	EWW, EWD, LWW, LWD	Schweingruber, F.H. (2002-05-28): NOAA/WDS Paleoclimatology - Schweingruber - Tschokurdach, Ochotingna - LAGM - ITRDB RUSS142. NOAA National Centers for Environmental Information. https://doi.org/10.25921/kxgc-s381. Accessed 2024-05-04.
RUSS143	63.67 N, 159.95 E	700 m	LAGM	EWW, EWD, LWW, LWD	Schweingruber, F.H. (2002-05-28): NOAA/WDS Paleoclimatology - Schweingruber - Kubaka right bank middle - LAGM - ITRDB RUSS143. NOAA National Centers for Environmental Information. https://doi.org/10.25921/965d-bp93. Accessed 2024-05-04.

RUSS144	61.17 N, 153.97 E	-	LAGM	EWW, EWD, LWW, LWD	Schweingruber, F.H. (2002-05-29): NOAA/WDS Paleoclimatology - Schweingruber - Julietta south - LAGM - ITRDB RUSS144. NOAA National Centers for Environmental Information. https://doi.org/10.25921/s4f4-jr90. Accessed 2024-05-04.
RUSS145	65.8 N, 137.25 E	800 m	LAGM	EWW, EWD, LWW, LWD	Schweingruber, F.H. (2002-05-28): NOAA/WDS Paleoclimatology - Schweingruber - Adycha river (slope) - LAGM - ITRDB RUSS145. NOAA National Centers for Environmental Information. https://doi.org/10.25921/qtdw-va05. Accessed 2024-05-04.
RUSS146	65.8 N, 137.25 E	800 m	LAGM	EWW, EWD, LWW, LWD	Schweingruber, F.H. (2002-05-29): NOAA/WDS Paleoclimatology - Schweingruber - Adycha river (bog) - LAGM - ITRDB RUSS146. NOAA National Centers for Environmental Information. https://doi.org/10.25921/qtjt-va17. Accessed 2024-05-04.
RUSS147	62.13 N, 155.03 E	700 m	LAGM	EWW, EWD, LWW, LWD	Schweingruber, F.H. (2002-05-29): NOAA/WDS Paleoclimatology - Schweingruber - Balygichan Ebene - LAGM - ITRDB RUSS147. NOAA National Centers for Environmental Information. https://doi.org/10.25921/7e6q-9k27. Accessed 2024-05-04.
RUSS148	62.13 N, 154.58 E	600 m	LAGM	EWW, EWD, LWW, LWD	Schweingruber, F.H. (2002-05-28): NOAA/WDS Paleoclimatology - Schweingruber - Balygichan River - LAGM - ITRDB RUSS148. NOAA National Centers for Environmental Information. https://doi.org/10.25921/e0kr-dq77. Accessed 2024-05-04.
RUSS149	60.35 N, 154.12 E	200 m	LAGM	EWW, EWD, LWW, LWD	Schweingruber, F.H. (2002-05-28): NOAA/WDS Paleoclimatology - Schweingruber - Takhojama - LAGM - ITRDB RUSS149. NOAA National Centers for Environmental Information. https://doi.org/10.25921/e1vv-f658. Accessed 2024-05-04.
RUSS154	59.78 N, 154 E	80 m	LAGM	EWW, EWD, LWW, LWD	Schweingruber, F.H. (2002-05-28): NOAA/WDS Paleoclimatology - Schweingruber - Jama river - LAGM - ITRDB RUSS154. NOAA National Centers for Environmental Information. https://doi.org/10.25921/gdpt-9n83. Accessed 2024-05-04.

RUSS159	63.07 N, 76.32 E	170 m	LASI	EWW, EWD, LWW, LWD	Schweingruber, F.H. (2002-05-28): NOAA/WDS Paleoclimatology - Schweingruber - Under Vangapur River B - LASI - ITRDB RUSS159. NOAA National Centers for Environmental Information. https://doi.org/10.25921/9xxk-zt11. Accessed 2024-05-04.
RUSS162	69.53 N, 97.53 E	550 m	LAGM	EWW, EWD, LWW, LWD	Schweingruber, F.H. (2002-05-28): NOAA/WDS Paleoclimatology - Schweingruber - Ayakli River B - LAGM - ITRDB RUSS162. NOAA National Centers for Environmental Information. https://doi.org/10.25921/snpy-nr27. Accessed 2024-05-04.
RUSS163	71.7 N, 118.58 E	140 m	LAGM	EWW, EWD, LWW, LWD	Schweingruber, F.H. (2002-05-29): NOAA/WDS Paleoclimatology - Schweingruber - Ary-Ongorbynf-River B - LAGM - ITRDB RUSS163. NOAA National Centers for Environmental Information. https://doi.org/10.25921/ah2m-p719. Accessed 2024-05-04.
RUSS165	70.6 N, 104.25 E	130 m	LAGM	EWW, EWD, LWW, LWD	Schweingruber, F.H. (2002-05-29): NOAA/WDS Paleoclimatology - Schweingruber - Kotuykan River - LAGM - ITRDB RUSS165. NOAA National Centers for Environmental Information. https://doi.org/10.25921/a508-4r62. Accessed 2024-05-04.
RUSS166	71.9 N, 111.03 E	150 m	LAGM	EWW, EWD, LWW, LWD	Schweingruber, F.H. (2002-05-29): NOAA/WDS Paleoclimatology - Schweingruber - Popigay B - LAGM - ITRDB RUSS166. NOAA National Centers for Environmental Information. https://doi.org/10.25921/y1n6-3910. Accessed 2024-05-04.
RUSS178	64.83 N, 169 E	-	LAGM	EWW, EWD, LWW, LWD	Schweingruber, F.H. (2002-05-28): NOAA/WDS Paleoclimatology - Schweingruber - Markovo - LAGM - ITRDB RUSS178. NOAA National Centers for Environmental Information. https://doi.org/10.25921/bp2s-fp43. Accessed 2024-05-04.
RUSS179	64.83 N, 169 E	-	LAGM	EWW, EWD, LWW, LWD	Schweingruber, F.H. (2002-05-28): NOAA/WDS Paleoclimatology - Schweingruber - Markovo, junge Bäume - LAGM - ITRDB RUSS179. NOAA National Centers for Environmental Information. https://doi.org/10.25921/e914-gh70. Accessed 2024-05-04.

RUSS180	65.32 N, 64.65 E	30 m	LASI	EWW, EWD, LWW, LWD	Schweingruber, F.H. (2002-05-29): NOAA/WDS Paleoclimatology - Schweingruber - Muzhy-Settlement - LASI - ITRDB RUSS180. NOAA National Centers for Environmental Information. https://doi.org/10.25921/5aev-f807. Accessed 2024-05-04.
SWIT168	46.4 N, 7.43 E	1900 m	LADE	EWW, EWD, LWW, LWD	Schweingruber, F.H. (2002-05-28): NOAA/WDS Paleoclimatology - Schweingruber - Simmental, Iffigenalp - LADE - ITRDB SWIT168. NOAA National Centers for Environmental Information. https://doi.org/10.25921/7zjd-n118. Accessed 2024-05-04.

B1.2 | Binning and function building

All three functions for the model were build on binned data based on the independent variable. For the function construction it was decided to rely on average values from bins because of the great amount of data points and the high variability in data. Further the data showed biases in its distribution varying between the variables.

Table B2: Data bins for the three different functions constructed with binning of the observed, independent variables July-August Temperature (°C), growing season start as day of the year (DOY) and latewood density (kgC/m^3). Ranges give the range of observed values for which was binned in the specified intervals resulting in a certain number of bins and an average bins size. The bias in the data showing the necessity of binning is given by the range of the independent variable in which 80% of data points were.

	Binned, independent variable	Dependent variable	Range	Number of bins	Average bin size	Intervals	Range of 80% of data points
Latewood density function	July-August Temperature	Latewood density	3 °C - 20 °C	34	217	0.5 °C	8.56 - 13.15 °C (27.6%)
Phenology function	Growing season start	Earlywood width	DOY 71 - 172	96	71	1 day	DOY 128 - 156 (26.8%)
	Latewood density	Latewood width	225 - 455 kgC/m3	46	148	5 kgC/m3	267 - 361 kgC/m3 (40.8%)

The latewood density function models a LW-factor in response to July-August average temperatures. The LW-factor is a factor modifying a species-specific EW density to achieve the

respective LW density. By using the LW-factor rather than absolute LW density, the EW density differences between species could be accounted for. Out of all monthly average temperatures, July and August were the two single months with the highest correlations with LW density (Fig. B2). The July-August mean temperature was the period with the highest correlation overall which aligns with previous findings.

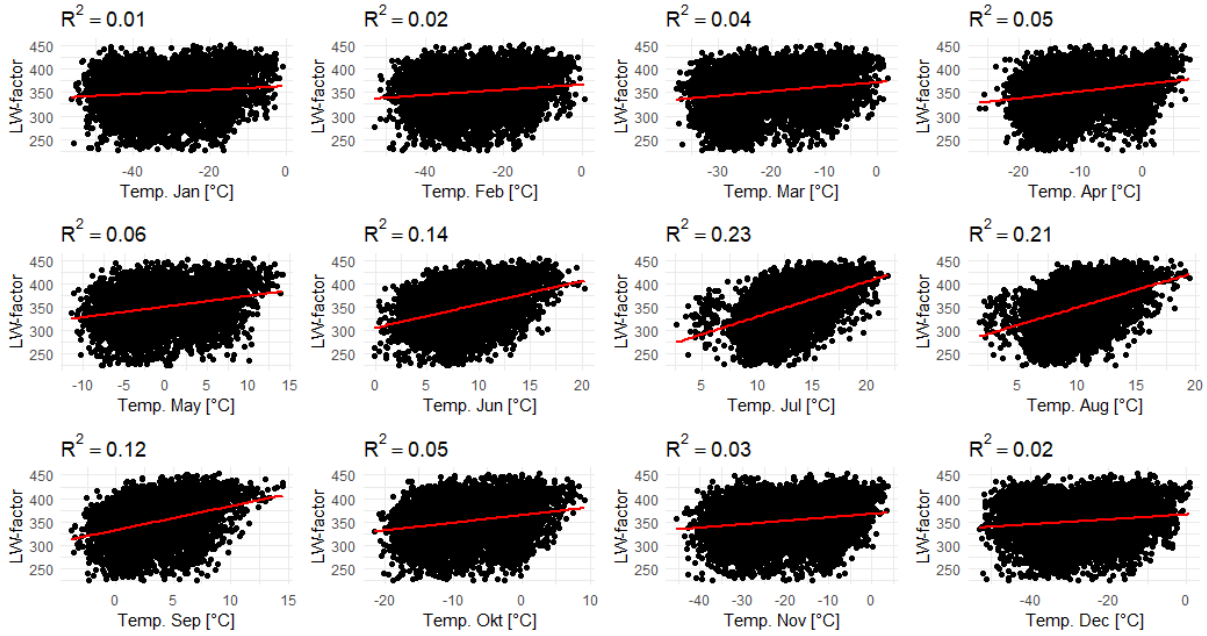

Figure B2: Comparison of the correlations between monthly average temperatures and the latewood density modification factor (latewood density/standrad earlywood density).

For the latewood density function, 80% of data points had summer temperatures between 8.56 °C and 13.15 °C corresponding to only 27.6% of the total temperature range (Fig. B4a). The EW density data per species was normally distributed with mean and median values close together so that the selection of the closest integer between those was reasonable as standard EW density (Fig. B3). The standard EW density was 167 kg C/m^3, 165 kg C/m^3 and 157 kg C/m^3 for European larch, Dahurian larch and Siberian larch respectively.

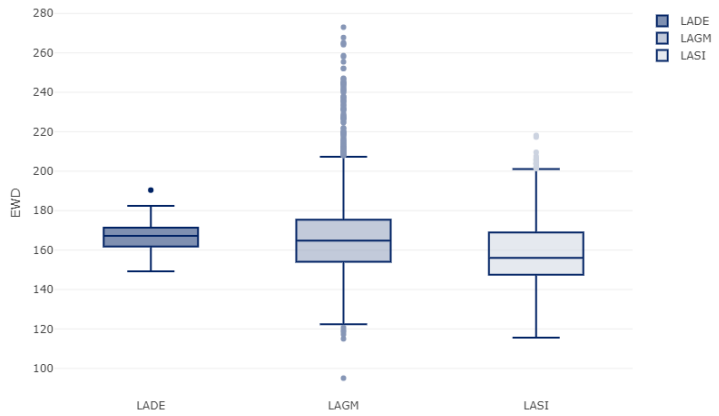

Figure B3: Earlywood density (EWD) distributions per species. LADE = European larch (*Larix decidua*), LAGM = Dahurian Larch (*Larix gmelinii*) and LASI = Siberian Larch (*Larix sibirica*).

To base the construction of the function on the effect of temperature alone as best as possible, bins were created and bin average LW density and temperature used as data for the function development. The binning strategy considered data in the temperature range of 3-20 °C and divided it into 34 bins of 0.5 °C intervals (Tab. B2). The bins average values were verified to be significantly different from each other using a one-way analysis of variance (F-value = 3658, p-value < 2^{-16}). The analysis of variance was used to verify that binning offers a representation of a trend in the observed data as it indicates an effect of temperature on the LW density.

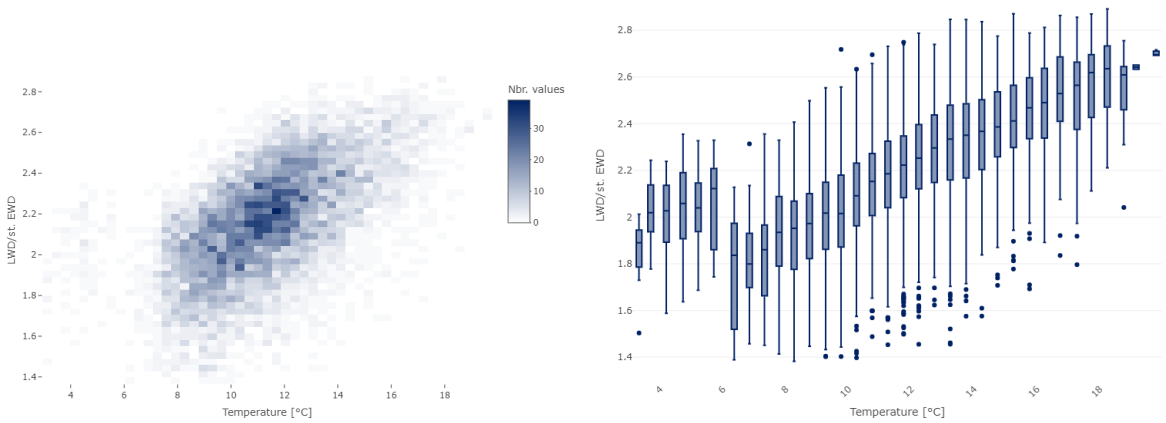

(a) Visualization of data point distributions to see bias in available data.

(b) Boxplots showing the latewood factor distribution in each bin.

Figure B4: Observed data from the ITRDB (National Oceanic and Atmospheric Administration (NOAA), 2022) of wood density used for the temperature-response function.

The automated lm-algorithm of R was used to find the best fit to the binned average values considering linear and quadratic functions. Relative stability outside the temperature-range of the bins was assumed, leading to the additional consideration of a fitted logistic growth curve

with implicit stability. The logistic growth curve was fitted based on the highest R^2. The best parameter value combination was found through a structured approach to testing all possible parameter combinations within preset ranges for each parameter. The preset ranges were set based on visual data inspection. For the final model the logistic growth function was chosen as it best incorporated the assumption of relative constant LW-factor values outside the range of observed temperature values.

Table B3: Comparison of the functions in respect to their performance in reproducing bin average latewood density

	Linear	**Quadratic**	**Logistic growth**
function	$1.64 + 0.05 * T$	$2.21 + 1.42 * T + 0.31 * T^2$	$1.35 + \frac{(2.8-1.35)}{1+e^{-0.21(T-10.2)}}$
R^2	0.87	0.91	0.86
RMSE (%)	4.28	4.28	6.24

The default phenology of the simple model was based on observed EW:LW width ratio. The slope of 0.43 is approxiamtely equal to a 70% EW and 30% LW part of the total tree ring width (Fig. B5). The phenology function consists of two functions for EW width and LW width

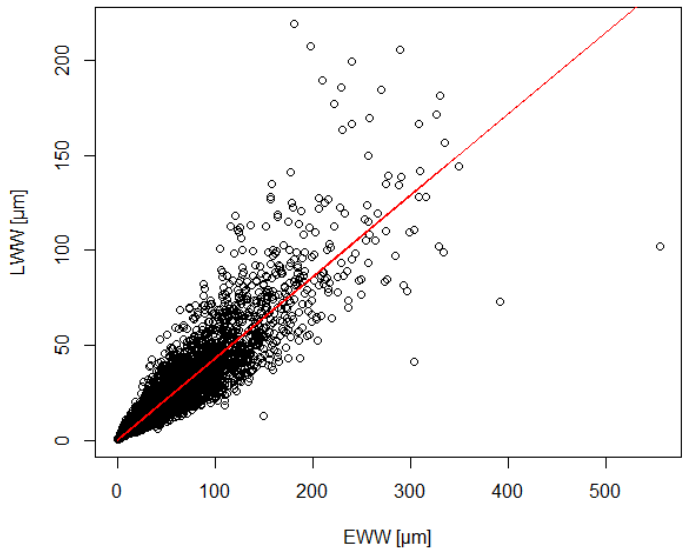

Figure B5: Observed earlywood width (EWW) plotted against observed latewood width (LWW) with the linear trend (red line) with a slope of 0.43 (R^2 = 0.91).

respectively. EW width is dependent on the growing season start of the stem. For modelling the

growing season start (*GSS*) we relied on the reported relationship of Cuny et al. (2019) for larch

$$GSS = 167.42 - 4.71 * T_a \tag{B2}$$

in which T_a, the mean annual temperature, is the driver for varying GSS dates. The data was binned with a bin for each unique GSS date resulting in 96 bins ranging from day of the year 71 - 172 as GSS date with on average 71 data points per bin (Tab. B2). The bins average differed significantly from each other as tested with a one-way analysis of variance (F-value = 227, p-value < 2^{-16}). 80% of data points had GSS dates between day of year 128 and 156 corresponding to only 26.8% of the total GSS range (Fig. B6a). The EW width is simulated with the function

$$EWW = 758.41 - 2.51 * GSS \tag{B3}$$

returning the EW width in μm.

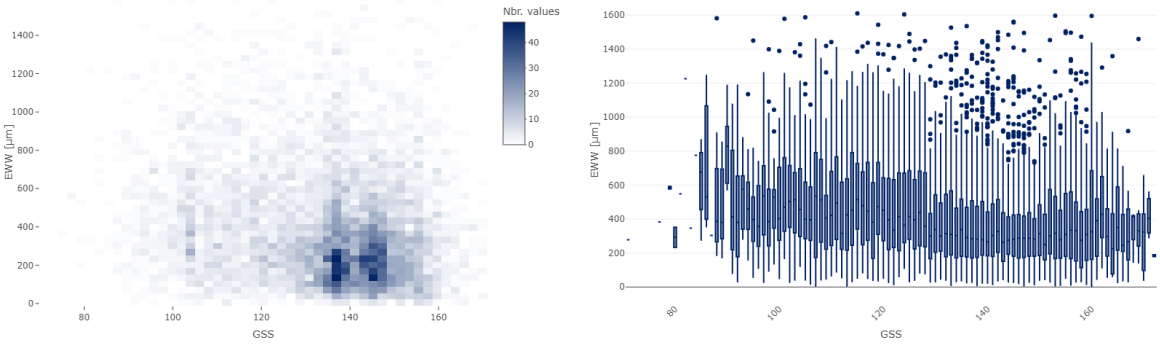

(a) Visualization of data point distributions to see bias in available data.

(b) Boxplots showing the latewood factor distribution in each bin.

Figure B6: Observed data from the ITRDB (National Oceanic and Atmospheric Administration (NOAA), 2022) of wood density used for the temperature-response function

The LW width is modelled in dependency of LW density. A non-linear relationship between the two variables was observed. For the LW width function, 80% of data points had LW density values between 267 and 361 kgC/m^3 corresponding to 40.8% of the total LW density range (Fig. B7a). LW density was binned into 46 bins in fixed intervals of 5 kgC/m^3 in the range of 225 to 455 kgC/m^3 with an average bin size of 148 data points (Tab. B2). The bins averages differed significantly from each other as tested with a one-way analysis of variance (F-value = 131015, p-value < 2^{-16}). An exponential growth function was fitted with the nls() function of R. The final function models LW width (*LWW*) dependent on LW density (*LWD*) through

$$LWW = 4.0832 * e^{0.0104 * LWD} \tag{B4}$$

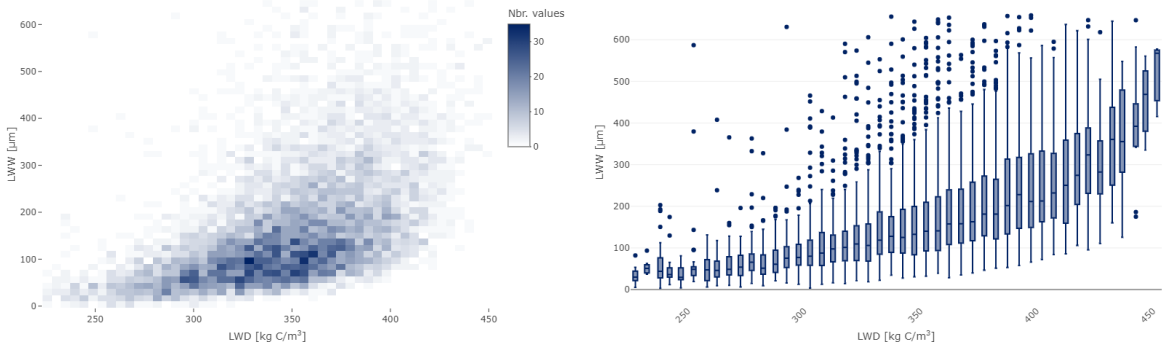

(a) Visualization of data point distributions to see bias in available data.

(b) Boxplots showing the latewood factor distribution in each bin.

Figure B7: Observed data from the ITRDB (National Oceanic and Atmospheric Administration (NOAA), 2022) of wood density used for the temperature-response function

B2 Supplementary Material to Results

Table B4: Mean observed and modelled tree ring densities at the four sites in Lötschental, Switzerland with the respective range and relative range of annual mean tree ring densities across the period of available observations. Modelled mean densities and absoult density ranges are given in kgC/m^3.

		Observed	Modelled (default phenology)	Modelled (emerging phenology)
N13D	mean	0.54	239.1	262.4
	range	0.47 - 0.63	232.8 - 244.2	242.1 - 278.6
	rel. range	87% - 116%	97% - 102%	92% - 106%
N13W	mean	0.50	238.7	260.7
	range	0.47 - 0.54	232.8 - 244.2	242.1 - 279.0
	rel. range	94% - 108%	98% - 102%	93 % - 107 %
S19D	mean	0.52	225.5	228.6
	range	0.49-0.55	218.4 - 233.2	211.7 - 248.3
	rel. range	94% - 105%	97% - 103%	93% - 109%
S22W	mean	0.49	213.9	206.9
	range	0.42 - 0.66	205.4 - 226.2	193.3 - 232.0
	rel. range	85% - 134%	96% - 106%	94% - 112%

Table B5: Mean observed and modelled tree ring densities at the four sites in Lötschental, Switzerland with the respective relative difference of annual mean tree ring densities to the mean value of the period of S22W. Modelled mean densities are given in kgC/m^3.

		Observed	Modelled (default phenology)	Modelled (emerging phenology)
N13D	mean	0.54	239.1	262.4
	relative to S22W	0%	0%	0%
N13W	mean	0.50	238.7	260.7
	relative to S22W	+ 6.12%	+ 5.42%	+10.49%
S19D	mean	0.52	225.5	228.6
	relative to S22W	+2.04%	+ 11.59%	+ 26.00%
S22W	mean	0.49	213.9	206.9
	relative to S22W	+ 10.00%	+ 11.73%	+26.63%